UNIVERSITÀ DEGLI STUDI DI TRIESTE

XXIX CICLO DEL DOTTORATO DI RICERCA IN

NANOTECHNOLOGY

Fabrication of 3D micro-objects by two-photon lithography for optical tweezers manipulation

Settore scientifico-disciplinare: FIS/03 FISICA DELLA MATERIA

DOTTORANDA
FARIDEH ABHARI

COORDINATORE
PROF. LUCIA PASQUATO

SUPERVISORE
DR. MASSIMO TORMEN

TUTORE
DR. DAN COJOC

ANNO ACCADEMICO 2015/2016

Fabrication of 3D micro-objects by two-photon lithography for optical tweezers manipulation

Abstract

In the last decade Optical Tweezers (OT) and Two Photon Polymerization (TPP), two already established techniques for contactless manipulation of micro-objects in liquids and for the fabrication of three-dimensional micro-objects of arbitrary shape, respectively, have consolidated their presence in the laboratory practice, not only as subject of scientific and technical investigations, but also as convenient tools for applications to other fields.

This thesis tries to combines these worlds, using TPP to fabricate micro-objects that could be trapped and actuated by OT, with the aim of pushing forward the possibilities of producing new tools, in particular for cell biology studies. We demonstrated here a convenient scheme for the fabrication of 3D micro-objects by two-photon lithography, their release from the substrate under physiological conditions and actuation by optical tweezers. This opens interesting possibilities in mechanobiology experiments, for fabricating and precisely placing 3D micro-tools in proximity with living cells and actuating them by optical tweezers (OT) to operate on cells. These possibilities can be extended to the simultaneous dynamical manipulation of more trapped objects as demonstrated in recent years.

In the present work micro-objects with and without mirror-symmetry were fabricated by two photon lithography (TPL) in SU-8 negative photoresist on a water soluble sacrificial layer on glass, released from the substrate in water, and set into rotational motion by optical tweezers, exploiting the optically induced torque generated by a focused laser beam interacting with micro-objects with broken mirror-symmetry.

While fabricated simple micro-cones were found stable in the optical trap, micro-cones modified with the addition of chiral features were propelled away due to the imbalance of scattering, gradient optical forces and fluid dynamic forces generated in the rotation.

In the near future the combination of optical tweezers, two-photon polymerization and advanced imaging techniques will enable new studies of the effects of mechanical stimulation of a cell onto the molecular events inside the cell.

Abstract

In questo ultimo decennio, gli Otpical Tweezers (OT) e la tecnica della Two Photon Polymerization (TPP), tecniche già conosciute rispettivamente per la manipolazione di non-contatto di micro-oggetti in liquidi e per la fabbricazione di micro-oggetti tridimensionali di forma arbitraria, hanno visto un consolidamento della presenza nella pratica di laboratorio, non solo come soggetto di studio tecnico-scientifico, ma anche come utili strumenti per applicazioni in altri campi.

In questa tesi si tenta di combinare questi due mondi, usando la TPP per la fabbricazione di micro-oggetti da intrappolare poi con gli OT, con l'obiettivo di dare un'impulso alle possibilità di produrre nuovi strumenti per studi, in particolare nel campo delle biologia cellulare.

Questo lavoro dimostra un utile schema di fabbricazione di micro-oggetti 3D con la litografia a due fotoni, la loro separazione dal substrato in condizioni fisiologiche, ed attuazione con gli optical tweezers.

Questo consente di condurre nuovi esperimenti di meccano-biologia, grazie alla fabbricazione e al posizionamento preciso di micro-oggetti 3D in prossimità di cellule vive, e la loro attuazione con gli optical tweezers, in modo da operare sulle cellule.

Queste possibilità potranno essere ulteriormente estese grazie alla capacità di manipolare dinamicamente più oggetti intrappolati, come dimostrato in anni recenti.

Nel presente lavoro micro-oggetti con o senza simmetria di parità sono stati fabbricati mediante litografia a due fotoni nel resist negativo SU-8, depositato su uno strato sacrificale steso su vetro. Successivamente tali micro-oggetti sono stati rilasciati dal substrato dissolvendo lo strato sacrificale in acqua, e messi in rotazione con gli optical tweezers, sfruttando il momento torcente sviluppato dall'interazione del fascio laser con i micro-oggetti con simmetria di parità rotta.

Mentre semplici micro-coni sono risultati stabilmente intrappolati con gli optical tweezers, micro-coni modificati con l'inserimento di strutture chirali, sono sospinte fuori dalla trappola ottica, per lo sbilanciamento tra le forze di scattering, le forze di gradiente ottico e le forze fluido-dinamiche generate dalla rotazione.

In un prossimo futuro la combinazione di optical tweezers, two-photon polymerization e di tecniche di imaging permetterà di condurre nuovi studi dell' effetto della stimolazione meccanica di cellule sugli eventi molecolari che avvengono al loro interno.

Acknowledgements

I would like to express my special appreciation and thanks to the people who have helped to make this work possible.

Firstly, I want to express my sincere gratitude to my supervisor Dr. Massimo Tormen for the continuous support of my Ph.D study and related research, for his patience, motivation, and immense knowledge. His guidance helped me in all the time.

I am also grateful to PhD coordinator in Nanotechnology department, Prof. Lucia Pasquato for her patience and support in overcoming numerous obstacles I have been facing through my research.

I wish to thank my advisor, Dr. Dan Cojoc, for giving me the unique opportunity to work in Bio-Lab with an excellent group, and many important research suggestions.

My sincere thanks also goes to Dr. Miltcho Danailov and Electromagnetism group for providing me Laser facilities, and who gave access to the laboratory and research facilities. Without they precious support it would not be possible to conduct this research.

Another person which I want to thank is Dr. Solaiman Yousafzai . He believes in me even if he wasn't always very satisfied of what I was doing. I thank for his invaluable guidance, patience, and friendship throughout all my work.

I would like to thank my fellow doctoral students for their feedback, cooperation and of course friendship. In addition I would like to express my gratitude to the staff of Physics department.

I would like to thank my family: my parents and to my brother and sisters for supporting me spiritually throughout writing this thesis and my life in general.

Declaration

I hereby declare that this Ph.D. thesis entitled "**Fabrication of 3D micro-objects by two-photon lithography for optical tweezers manipulation**" was carried out by me for the degree of **Doctor of Philosophy** in English under the guidance and supervision of **Dr. Massimo Tormen**, Faculty of Physics, Department of Nanotechnology, University of Trieste, Italy.

Place: Trieste -Italy Farideh Abhari

Date: December 2016

ABSTRACT i
ABSTRACT ii
ACKNOWLEDGEMENTS iii
DECLARATION iv
LIST OF FIGURES ix

CHAPTERS

1 INTRODUCTION 1

1.1 Two-Photon Photopolymerization and 3D Lithographic Microfabrication 1
1.1.1 Photoinitiation and Photopolymerization 1
1.1.2 Photopolymerization Induced by Two-Photon Absorption 4
1.1.3 Material Processing with Femtosecond Lasers 6
1.1.4 Femtosecond Laser 3D Micro-Nanofabrication 7
1.1.5 Design Consideration of Optical Setup 7
1.1.6 Applications 9
1.1.7 The Development of Micro-Scale Lithographic Techniques 10

1.2 Optical Tweezers 10
1.2.1 Principles of Optical Trapping in Biological Field 11
1.2.1.1 Explanation of the Optical Force 11
1.2.1.2 Theoretical Determination of the Torque 12
1.2.2 General Study for Single-molecule Manipulation 13
1.2.3 Technical Requirements 13
1.2.4 Biological Applications 14

1.3 Motivation and Problem Statement 15

1.4 Research aim and Objectives 16

1.5 Method Statement 17

1.6 Dissertation Outline 18

2 MATERIALS AND METHODS 20

2.1 Two-Photon Microfabrication System 20
2.1.1 Laser Specification 20
2.1.2 Optical Setup 20
2.1.3 Software Development and Computer Control 22
2.1.4 Photoresists Material 23
2.1.5 Sample Preparation 24
2.1.6 Characterization of the System 25

2.2 Optical Trapping and Manipulation 26
2.2.1 Optical Tweezers Vertical Indentation Setup 27
2.2.2 Calibration of the Optical Trapping 29
2.2.3 OT Set-up Sensitivity 30
2.2.4 Trap Stiffness Determination 30
2.2.5 Optical Rotation and Torque 32

3 RESULTS AND DISCUSSION 33

3.1 Two-Photon Microfabrication Performance 33
3.1.1 Spatial resolution in polymerization 33
3.1.2 Fabrication and Optimization of Asymmetrical Objects 38
3.1.2.1 Cone-Shaped Objects 41
3.1.2.2 3D Micro-structures with Hollow Channels 42

3.2 Mechanical and Optical Manipulation of Mirco-Objects 45
3.2.1 Stuck Micro-Object Calibration 46
3.2.1.1 Voltage Versus Position Calibration 46
3.2.1.2 Position Distribution Recording 50
3.2.2 Measurement of the Trap Stiffness 51
3.2.3 Data Analysis and Explanation 51

3.3 Rotation and the Corresponding Torque Generated by the 3D Micro-Object 53

3.3.1 Change of rotation speed with power and type of asymmetry 54
3.3.2 Micro propeller and circling objects 55
3.4 Discussion 56

4 CONCLUSION AND RECOMMENDATIONS FOR FUTURE RESEARCH 59

4.1 Summary 59
4.2 Conclusion 60
4.3 Future Research 60

BIBLIOGRAPHY
APPENDICES

List Of Figures

Fig. 1.1 Schematic shows the atom excitation process with : a) Single-photon absorption; b) Stepwise absorption of two photons; c) Two-photon absorption(TPA)

Fig. 1.2 A crossbeam two-photon two-color scanning laser microscopic system(Sun and Kawata, 2004).

Fig. 1.3 Two-photon direct writing laser microfabrication system(Sun and Kawata, 2004)

Fig. 1.4 the origin of the trapping force(Moffitt et al., 2008)

Fig. 2.1 TPP experimental setup; L1 and L2 lenses for beam expander, L3 imaging tube lens, DM – Dichroic Mirror, OBJ – microscope objective

Fig. 2.2 Experimental setup consisting of a Femtosecond (fs) laser, a XYZ piezo-driven stage for 3D scannig the sample, beam expander, microscope objective and other optical elements on a frame mounted on a stable anti-vibration optical table.

Fig. 2.3 Different sample configuration for solid and liquid photoresists(Serbin et al., 2004)

Fig. 2.4 Sample preparation and fabrication process of micro-objects. There are four main steps: i) sacrificial layer spin coating on clean cover glass, ii) SU-8 spin coating on sacrificial layer, iii) exposure and development of photoresist, iv) adding water or physiological solution to release structures from the PVA sacrificial layer and trap them by (OT) set-up

Fig. 2.5 Depth of focus (DoF) is determined by the distance from the nearest object plane in focus to that of the farthest plane simultaneously in focus (Olympus Microscopy Resource Center).

Fig. 2.6 Optical tweezers setup for trapping 3D mico object. (a) Laser trapping beam path (red) and bright-field imaging path (green). PS: 3-axis nano-piezo stage; DAQ: digital analog acquisition card; TL: tube lens; L1-L3 convergent lenses; M1-M3: mirrors; DCM 1-2 dichroic mirrors, TC: temperature controlled holder (b) Interference pattern imaged on the QPD for: equilibrium position, lateral and axial displacements(Yousafzai et al., 2016).

Fig. 2.7 Changing the relative positions of the two lenses of the beam expender, one can increase or decrease the width of the beam as well as the trap location relative to the objective's focal plane (dotted line)(Yousafzai et al., 2016).

Fig. 2.8 Trace of thermal Brownian motion of a trapped bead from the QPD in volts. The plot is a section (1 sec) of 5 sec trace sampled with 10 kHz.

Fig 2.9 (a) The stage with a stuck bead is moved sinusoidally with a 1μm of amplitude, with trap focus is at the middle of the bead, and the QPD response is monitored. (b) By plotting the linear part of stage displacement and QPD voltage signal we get the QPD sensitivity as V/μm(Yousafzai et al., 2016).

Fig. 2.10 The Gaussian distribution is a general mathematical distribution.

Fig. 3.1 SEM image of a row of voxels polymerized at the same power condition but with different focusing height.

Fig. 3.2 Adjusted laser focus point with the highest intensity under CCD camera.

Fig. 3.3 SEM image for 3D Helix fabricated by two photon lithography at 400 μw for two different exposure times (5ms, 10 ms, left and right, respectively).

Fig. 3.4 SEM image for 3D Helix fabricated by two photon lithography at 300 μw and 5 ms exposure time.

Fig. 3.5 SEM image for 3D Helix fabricated by two photon lithography at 300 μw and 3 ms exposure time

Fig. 3.6 SEM image for 3D Helix fabricated by two photon lithography at 250 μw and 5 ms exposure time.

Fig. 3.7 SEM image for 3D Helix fabricated by two photon lithography at 600 μw and 20 ms expo with 1μm step size.

Fig. 3.8 Designed simple Cone in Rhino 4.

Fig. 3.9 Front Panel of the LabVIEW software, Activex Interface.

Fig. 3.10 Back diagram of the LabVIEW software, Activex Interface.

Fig. 3.11 A row of cone-shaped objects for optical trapping .

Fig. 3.12 Cylinder with about 2 μm cavity fabricated by TPL.

Fig. 3.13 Failed fabrication of cone with deep spiral cavity.

Fig. 3.14 Type (II) : Cone with 45 degree spiral cavity.

Fig. 3.15 Type (I) : Cone with 22 degree spiral cavity.

Fig. 3.16 A plot of the position sensitive detector voltage output corresponding to theamplitude of displacement 400 mW, in 3 X,Y and Z axis of a trapped cone relative to the centre of the trap.

Fig. 3.17 A plot of the position sensitive detector voltage output corresponding to the amplitude of displacement 200 mW, in 3 X,Y and Z axis of a trapped cone relative to the centre of the trap.

Fig.3.18 One trapped micro-cone (right) and one free cone (left) imaged by the CCD camera of the microscope. Observe that the symmetry axes of the trapped cone aligns with the propagation direction of the laser beam.

Fig. 3.19 The two previous cones after switching the laser beam off.

Fig. 3.20 The second cone is trapped, close to the free cone. Again the axes of the cone aligns with the beam propagation direction.

Fig. 3.21 Trapped symmetric cone position histogram in 3 axes (bell-curves)-The right side is at 200 mW power and the left at 400 mW.

Fig. 3.22 The height of the cone is about 12 μm. (a) Orientation of the cone in laser trap. The cone's barbed end is always oriented opposite to the direction of propagation of trapping laser. (b) The change in rotation speed with the focus of the trapping laser. The rotation is maximum when the focus lies at the center of the cone (location I).

Fig. 3.23 Optically induced rotation of chiral cones. The height of each cone is about 12 μm and the peak is less than 500 nm with 1 μm deep for spiral cavity in water. They rotate clockwise with the laser power between 100 to 1000 mW.

Fig. 3.24 Laser power as well as asymmetry dependence on rotation of cone. Different asymmetries produce different torques and hence the rotation.

Fig.3.25 The cone rotates in the trap in counterclockwise direction- in this image can be seen two frames after rotating the asymmetric cone . The rotating cone acts like a μ-propeller and circulate the fluid around it (frame one) and the ordinary shaped particle (encircled in green) follow the dotted path during cone rotation(frame two).

1 INTRODUCTION

1.1 Two-Photon Photopolymerization and 3D Lithographic Microfabrication

Fabrication of three dimensional (3D) micro- and nano-structures has always represented an essential limit of the other frequent lithographic techniques, like Electron-beam lithography and optical lithography(Sun and Kawata, 2004).

Two Photon Polymerization (TPP) offers a relatively new possibility for fabricating three-dimensional (3D) microstructures at the sub-micrometer scale resolution. Several researchers extensively studied the physics of this technique experimentally and theoretically, during the last decade(Inoue and Ohtaka, 2013). The great potential of modern femtosecond near-infrared laser for microfabrication has gained considerable attention over the past years due to following reasons: (a) near-infrared laser can fabricate complex and arbitrary 3D microstructures using computer generated 3D model; (b) the mechanism is coherent and repeatable; (c) 100 nm spatial resolution can be obtained; (d) Diverse 2D-3D microstructures can be integrated directly into complex experimental microdevices(Maruo and Fourkas, 2008).

The quadratic dependence of two photon absorption (TPA) on incident light intensity implies that photopolymerization is confined to the volume of the focal spot, while the dose threshold for the polymerization is not reached outside, both vertically and laterally, this region, offering the possibility for a 3D precise patterning(Lee et al., 2006).

By precisely controlling the movement of sample or beam focus position, the negative tone photoresist is fully solidified point by point (voxel by voxel) and unexposed areas are removed using a suitable solvent as developer, resulting in the formation of a 3D micro objects (floating in the solvent or anchored to the substrate, depending on whether the cross-linked polymer is disconnected or connected to the substrate)(Teh et al., 2005).

1.1.1 Photoinitiation and Photopolymerization

Photopolymerization is the process of inducing the formation of new chemical bonds between molecules leading to the formation of larger size (macro)molecules, by light in

infrared (IR), visible, ultraviolet (UV), extreme ultraviolet (EUV) or X-ray spectrum(Popmintchev et al., 2012).

Light is used to provide the energy to bring monomers and oligomers in an excited state, initiating a series of chemical reactions leading to the formation of new bonds(Cicero et al., 2002).

The solidification process can be obtained in two ways; polymerization and cross-link. Polymerization is a chemical reaction in which small and simple molecules or monomer linked together to create macromolecule with several times larger molecular weight compared to the original molecule while cross-link is a bond that links one polymer chain to another. In addition to radiation the above reactions can be initiated by heat, pressure, change in pH(Chen, 2002).

The main difference between these two chemical reactions is in their quantum yield, which is defined as the ratio of polymerized monomer's unit number to the number of photons absorbed. In photo-cross-linking, addition of each monomer unit requires absorption of a photon(Kuckling et al., 2002), since all photons are not absorbed productively, the typical quantum yield will be less than 1(Semonin et al., 2011); on the contrary, photo-polymerization is represented via chain reactions so quantum yields greater than 1 are possible as shown in the following equation:

$$M \xrightarrow{M} M_2 \xrightarrow{M} M_3 \ldots M_{n-1} \xrightarrow{M} M_n \qquad (1.1)$$

where M is the monomer unit and M_n is the macromolecule containing n monomer units(Percec and Holerca, 2000). As mentioned above, the quantum yield can be in general low. For improving efficiency, low-weight molecules which are more sensitive to light added to photopolymer. These small molecules are called photoinitiators and when exposed to radiation, create reactive species like free radicals or actions. Photocurable materials are formed through this proceeding in three steps: initiation, chain propagation and chain termination(Madou, 2002).

For instance, when a Photoinitiators (I) absorb suitable photon energy, it is transformed into an intermediate state of the photoinitiators (I*) and free radicals (R·) are generated in initiation step as following(Balta et al., 2007):

$$I \xrightarrow{h\nu} I^* \rightarrow R\cdot \qquad (1.2)$$

Accordingly, the polymerization process is explained by chain propagation step:

$$R\cdot + M \rightarrow RM\cdot \xrightarrow{M} RMM\cdot \ldots \rightarrow RM_n\cdot \tag{1.3}$$

The photo-induced radicals react with active monomers to create growing polymeric chain radicals(Ma et al., 2000). The chain termination reaction usually proceeds when two chain radicals are joined together:

$$RM_n\cdot + \cdot M_mR \rightarrow RM_nM_mR \tag{1.4}$$

or through disproportionation, which occurs when an atom like hydrogen is relocated from one radical chain to another resulting in two polymeric chains(Ebewele, 2000):

$$RM_n\cdot + \cdot M_mR \rightarrow RM_n + M_mR \tag{1.5}$$

There are two general reactions for photoinitiation: free radical and ionic. The above descriptions of polymerization are based on radical initiators. Particularly, there are two types of photopolymerization reactions which require triggering by different initiators and using for laser fabrication:

1) Double-bond addition of acrylates (radical-type)

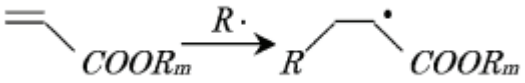

For a radical type initiator, benzoyl group chromophore is widely used since it exhibits good absorption in the UV region. Radicals are produced by different photochemical conversion processes like photoscission, intermolecular hydrogen abstraction and electron and proton transfer. For instance, an efficient radical initiator developed via bond cleavage is(Decker et al., 2001):

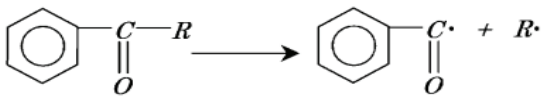

2) Ring-opening of epoxide (cationic-type)

Cationic photopolymerization is used less than the radical type. Cationic polymerization is a type of chain growth polymerization in which a cationic initiator transfers charge to a monomer which then becomes reactive. This reactive monomer goes on to react similarly with other monomers to form a polymer. In addition, cationic polymerization

reactions are very sensitive to the type of solvent which is used. Cationic ring-opening polymerization follows the same mechanistic steps of initiation, propagation, and termination. The photoinitiation is generally based on the ring opening of the Ethylene oxide, properly called oxirane(Solladié-Cavallo et al., 2005):

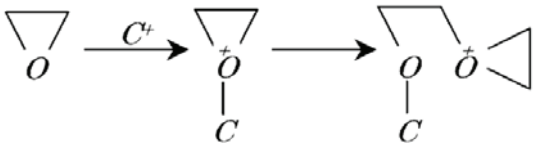

Compared to radical type reactions, the most important features of cationic polymerizations are low curing speed, lower viscosity and small shrinkage after polymerization. The essential information mentioned above is instructive for choosing a suitable material for laser fabrication(Shenoy, 2013).

Monomers have a much smaller molecular weight and consist of one or several reactive groups; they polymerize similarly to oligomers which is an important factor to determine the efficiency of polymerization(Ito et al., 1991). After polymerization, the oligomer composes the backbone of the polymer network. The physical, chemical and mechanical properties of the solidified resin strictly depend on the nature and structure of the oligomer. Particularly in 3D micro-nanolithography, suitable viscosity is important because of the opposite requirements in different steps of processing: a high viscosity is needed to avoid the drifting of small cross-linked volumes during exposure, on the contrary, low viscosity helps to remove unsolidified resin easily from recesses during development. In general, for what concerns other resist properties, lower shrinkage after polymerization, fast reaction time, high efficiency and low dark polymerization of active radicals at post-exposure are the preferred behaviors for a flawless fabrication(Ikada and Tsuji, 2000).

1.1.2 Photopolymerization Induced by Two-Photon Absorption

Excitation occurs when the absorbed photon energy matches the energy gap between the ground and excited states. Two-Photon Excitation (TPE) is a nonlinear absorption of two photons the total energy of which is sufficient to induce a molecular transition to an excited state. In conventional single-photon (λ) technique, UV or visible light have been used to excite fluorescent molecules of interest, the excited state is defined by the energy level (S_e) and the absorption rate measure linearly with the light intensity. However, exposure can undergo similar reactions when two photons (2λ) providing the

enough light intensity by simultaneously or sequentially (stepwise) absorption as shown in Figure (1.1)(Valeur and Berberan-Santos, 2012).

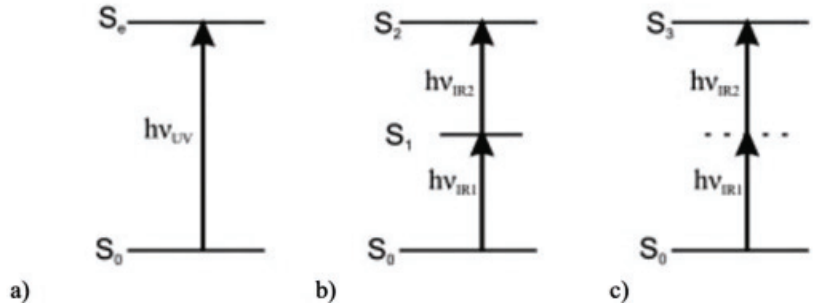

Fig. 1.1 Schematic shows the atom excitation process with : a) Single-photon absorption; b) Stepwise absorption of two photons; c) Two-photon absorption(TPA)

Quantum mechanically, a single-photon excites the molecule to an intermediate state, further promoted to a higher energy level by absorbing a second photon.

Through sequential absorption with resonant intermediate state (S_1), the first photon ($h\nu_{IR1}$) is absorbed by atom which can be characterized by a relaxation time or the specific lifetime of the energy level and before this excited level fades, the atom can be pumped to another excited state (S_2) by absorption of a second photon ($h\nu_{IR2}$). Therefore, sequentially absorption is mediated by a "real" energy state. The energies of both photons ($h\nu_{IR1}$, $h\nu_{IR2}$) are well defined can be unequal(Deiglmayr et al., 2008).

Two-photon Absorption (TPA) is the simultaneous absorption of two photons to transcend the energy gap in one excitation event. TPA is mediated by virtual states. Another difference is that the energy level of virtual excited state is not defined. Two-photon absorption is a third-order process and the atomic transition rate is proportional to the square of the light intensity, as a result, it is a nonlinear optical process(Sun and Kawata, 2004).

TPA was theoretically proposed as early as 1931 by Maria Göppert-Mayer in one of her doctoral dissertation and reported experimentally about thirty years later after the invention of the laser by Y-H Pao and P. M. Rentzepis as the fundamental work of multiphoton excitation induced photochemical reactions in 1965(LaFratta et al., 2007).

1.1.3 Material Processing with Femtosecond Lasers

Owing to the low beam quality and irreproducibility of the early lasers, after the first demonstration of the laser in 1960, the experiments mainly focused on simple research like material evaporation. Afterwards different types of lasers were developed like tunable solid ultrashort pulsed laser (Titanium: sapphire laser) in 1990 and resulted new areas of research like controlling, manipulating and processing of biological species in Micro/Nano scale and nonlinear optical microscopy. Ti:sapphire, emitting red and near-infrared light in the range from 650 to 1100 nanometers, can deliver pulses between a few picoseconds down to 10 femtoseconds and is tunable over as much as 400 nm (680-1080 nm). Other types of lasing material can be used which ensure power and frequency stability and high pulse power(Chichkov et al., 1996).

The energy and momentum are exchanged between the optical fields and molecules through absorption and emission. In this process, the imaginary part of nonlinear susceptibility represents the energy transfer from the light field to a medium. The light-matter energy change per unit time and unit volume is(Cohen-Tannoudji and Guéry-Odelin, 2011):

$$\frac{dW}{dt} = \left\langle \vec{E}.\dot{\vec{P}} \right\rangle \tag{1.6}$$

where $\vec{E}$ is the electric field vector and the brackets denote time average. The value of material polarization $\dot{\vec{P}}$ is:

$$P = \chi^{(1)}E + \chi^{(2)}E^2 + \chi^{(3)}E^3 + \ldots \tag{1.7}$$

where $\chi^{(i)}$ is susceptibility of the i^{th} tensor and $\chi^{(1)}$, $\chi^{(2)}$, $\chi^{(3)}$ are representing linear, second-order and third-order optical susceptibilities. For the centro-symmetric molecule systems, absorbing two photons with the same frequency, the even-tensors susceptibilities like $\chi^{(2)}$ and $\chi^{(4)}$ do not contribute to the resonant process. In centro-symmetric molecules the transition from S2 to S0 is symmetry forbidden for one photon, therefore the transition dipole moment for this transition is close to zero and the coupling between the ground and the excited state is very small, resulting in a long

radiative lifetime of the excited state. However even if the molecule was not centro-symmetric, the internal conversion relaxation from a higher-lying excited state is generally so fast that there still would not be fluorescence from S2 (or Sn). Therefore, the nonlinear absorption is described by the imaginary parts of $\chi(1)$, $\chi(3)$, of which typical effects are two photon and three-photon absorptions, respectively. The third-order susceptibility, $\chi^{(3)}$ is the sum of the nonlinear refraction ($\chi^{(3)}_{Real}$) and the nonlinear absorption ($\chi^{(3)}_{Imaginary}$). The imaginary part of the third-order susceptibility is related with two-photon absorption of the materials(Barrett and Grizzle, 1999).

The absorption rate of energy is described as follow:

$$\frac{dW}{dt} = \frac{8\pi^2\omega}{c^2 n^2} I^2 \operatorname{Im}\left[\chi^{(3)}\right] \tag{1.7}$$

where n is the refractive index, ω the incident light optical frequency, c the speed of light in vacuum, I the intensity of the light. In this equation, as has been point out, the TPA rate quadratically depends on the light intensity, which is an essential parameter for the spatial resolution in two-photon fabrication(Lakowicz, 2013).

1.1.4 Femtosecond Laser 3D Micro-Nanofabrication

In the past few years, many studies have been conducted on microscale fabrication technology using two-photon polymerization (TPP) with a femtosecond laser. TPP has many advantages specially for the direct fabrication of complex 3D structures on a scale of several microns, which is very complicated to obtain using conventional miniaturization technologies. In this technique, a femtosecond laser pulse is focused precisely onto liquid state monomers to initiate radical polymerization of the material and as a result. During exposure, a small volume around the center of the focused beam gets solidified as a result of the absorption of the threshold energy for polymerization. Therefore, deep sub-200 nm resolution structures can be obtained using a high Numerical Aperture (NA) objective lens. In recent years, researches have been mostly focused on the fabrication of precise 3D microstructures by employing various methodologies for specific applications(Lee et al., 2006).

1.1.5 Design Consideration of Optical Set-up

The first 3D optical set-up was proposed by Parthenopoulos and Rentzepis. In this configuration, a cross-beam of two-color and two- photon excitation was considered

but in this system was difficult to align the optical components and to synchronize the laser pulses. Nevertheless, the diameter of the volume at the coincidence point of the two beams focuses can be relatively small in this design. Later in 1990, Denk et al. in succeeded in applying two-photon excitation to laser scanning microscopy. Two-photon microscopy is a nonlinear microscopy type for three-dimensional imaging. In this set-up, two ultra-short pulses laser after beam splitter should overlap in both time and temporal domains for TPA process launched by simultaneously absorption of two photons as shown in figure 1.2.

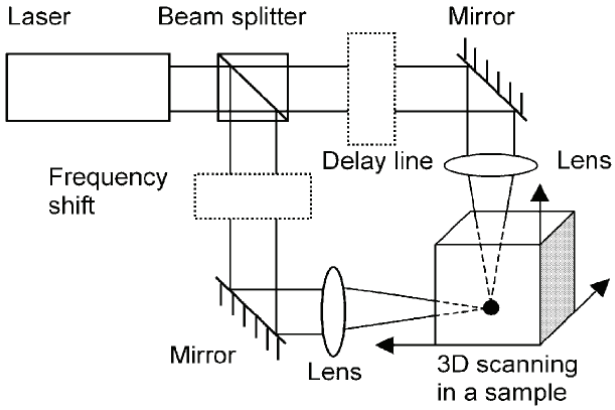

Fig. 1.2 A crossbeam two-photon two-color scanning laser microscopic system(Sun and Kawata, 2004).

This configuration was widely used due to its simplicity and has been taken as the standard for two-photon fluorescence microscopy. Now most two-photon photopolymerization systems take the form of a laser scanning microscope with enhanced 3D scanning capability(Sun and Kawata, 2004).

Figure 1.3 shows a typical set-up of a two-photon photopolymerization which consists three main steps; (i) 3D design and movement control during scanning, (ii) beam control, (iii) two-photon exposure and real-time monitoring. Laser beam focusing by a microscopic objective lens, is the most important issue to the entire fabrication system. High resolution of 3d micro-structure mostly depends on laser power and numerical aperture (NA) of objective lens. In addition, shorter wavelength will proportionally reduce the diffraction limit and focal spot size(Cumpston et al., 1999).

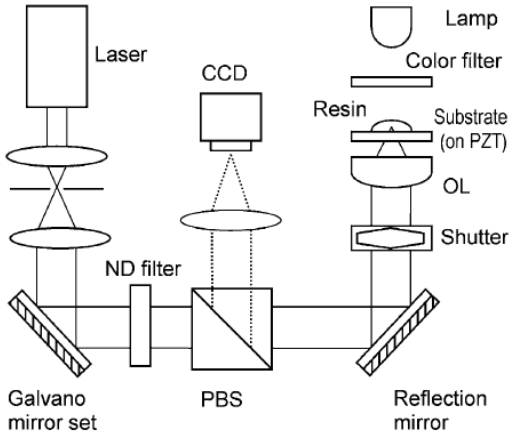

Fig. 1.3 Two-photon direct writing laser microfabrication system(Sun and Kawata, 2004).

After the laser focal spot is focused into resin, it should be scanned relatively to the sample using two possible means; a precise Lead Zirconate Titanate (PZT) XYZ piezoelectric stage can be used for moving in 3 different directions, although in some configuration, the Galvano mirror is used for scanning the laser beam in X-Y direction plus a PZT stage for Z axis. The polarization beam splitter (PBS) passes the laser beam but reflects the illumination light to the CCD camera for real-time monitoring of the fabrication process(Sun and Kawata, 2004).

1.1.6 Applications

Most of the work has been done in the field of optics, applications in medical devices and microelectronics are rapidly emerging. One of the most developed application in optics is the microfabrication of three-dimensional photonic crystals. A photonic crystal is a periodic optical nanostructure that affects the motion of photons in much the same way that ionic lattices affect electrons in solids. In biology, TPP has been used for cross-linking proteins on artificial substrates and inside living cells. Since these patterns retain enzymatic activity after laser processing, TPP is being considered for the fabrication of drug delivery devices on the micrometer scale. Other applications of TPP in the area of medical devices are the fabrication of three-dimensional scaffolds for tissue engineering by employing biocompatible materials as photoresists and the fabrication of tools for cell manipulation. Micro-tweezers and micro-needles were fabricated by TPP and remotely controlled via optical trapping with far greater precision than standard electrostatic devices. The surface of the microstructures fabricated by TPP can be chemically modified to enhance affinity toward metallic nano particles which led to the

formation of conductive three-dimensional structures. At the end, devices almost impossible to fabricate by standard lithography techniques now can be obtained by TPP(Eggers and Ehrlich, 1994).

1.1.7 The Development of Micro-Scale Lithographic Techniques

Shrinking the size of devices brings many advantages; more components per unit area, lower power consumption, lower cost, faster response and better performances. With the increasing complexity of micro/nano-devices and necessity to be compatible with many chemical and biological environments in most modern applications, there has been a tremendous effort from the research community to develop unconventional micro/nanofabrication techniques(Hennessy and Patterson, 2011).

1.2 Optical Tweezers

Optical tweezers (OT), basically called "single-beam gradient force trap", is a technique for contact-free manipulation of microscopic particles using light. A highly focused laser beam has been used to provide piconewton (pN) forces and depending on the refractive index mismatch to physically hold and move microscopic objects like. Accordingly, optical trapping offer great flexibility as a non mechanical contact tool often desired in biological experiments. This method is widely used in studying a variety of biological systems particularly the physical properties of single cells in recent years(Novotny et al., 1997).

The effect of light on material has been investigated for over four hundred years, Kepler's observed that comet tails always point away from the sun. Definitely, light from the sun can exert a pressure up to 5 mN/m^2 on a totally reflecting surface, ten orders of magnitude less than the force on a cube of the same dimensions due to gravity on the earth's surface(Osterbrock, 1958). Although resulting in an extremely small force, radiation pressure from sunlight can be significant, for example as the driving force behind solar sails where gravity is negligible. At the beginning of the twentieth century, using thin plates suspended in a evacuated radiometer, first, Lebedev measured experimentally the radiation pressure proposed by Maxwell-Bartoli, showing that the pressure for a reflective surface is twice that of an absorbing surface(Radenovic).

The detection of optical scattering and gradient forces on micron sized particles was first reported in 1970 by Arthur Ashkin. In 1987 he demonstrated trapping of living biological samples in a three-dimensional trap using a single Infrared laser beam.

Working in the lab of Arthur Ashkin at Bell Labs and then at the Stanford University, Steven Chu, used optical tweezing principles in his work on cooling and trapping neutral atoms earned the 1997 Nobel Prize in Physics, shared with Claude Cohen-Tannoudji and William D. Phillips(Chu, 1998).

Throughout the 1990s and afterwards, researchers used the optical trap force spectroscopy to characterize molecular scale biological motors. In the field of biology, the techniques of optical tweezers were applied in the field of cell-sorting in 2003. In this method, a large optical intensity pattern has been created over the sample area and cells sorted by their intrinsic optical characteristics accordingly(Dholakia et al., 2008).

1.2.1 Principles of Optical Trapping in Biological Field

The mechanical deformation characteristics of living cells are known to influence strongly their chemical and biological functions and the onset, progression and consequences of a number of human diseases. The mechanical responses of the cell during optical trapping to release the optical force have been analyzed to extract the elastic properties of the cell membrane by recourse to several different constitutive formulations of the elasticity and viscosity of the framework of a fully three-dimensional finite element analysis. A parametric study of various geometric, loading and structural factors is also undertaken in order to develop quantitative models for the mechanics of deformation by means of optical tweezers. Optical trapping is widely used to manipulate and measure with high precision different cellular structures in biophysics and also to perform some experiments in biology like cell sorting and single cell analysis. Researchers focus now, is on the basic science behind how force is generated in an optical trap and how it can be calibrated for characterization of the force spectroscopy in the biology field(Suresh et al., 2005).

1.2.1.1 Explanation of the Optical Force

The technique of optical manipulation has been employed as a unique means of controlling micro-dynamics of small objects without physical contact. Dielectric particle like a glass or polystyrene bead placed in proximity of the focus of a laser beam are subject to a gradient force. Optical force tends to push it towards the laser focus where the light intensity is higher. In fact, light carries a momentum and the net effect of the refraction by the object on the focus is a force that deflects some of this momentum away from the centre of the trap(Grier, 2003). By Newton's third law an equal and

opposite force must act on the object, pushing it towards the centre of the trap as it shows in figure (1.4a) and a similar refraction-related effect also causes the object to push back in the opposite direction of the laser beam (figure 1.4b). The trapping is stable only if the force of the laser light scattering from the particle toward the positive z–direction is compensated by a trapping force along the negative z-direction. To achieve this, a very tight focus is needed, with a significant fraction of the incident light coming in from large angles which is possible with a high numerical aperture objective lens(Moffitt et al., 2008).

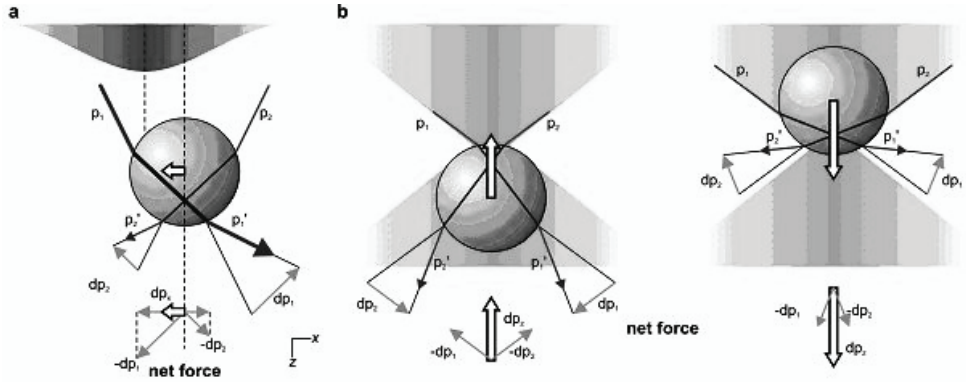

Fig. 1.4 the origin of the trapping force(Moffitt et al., 2008)

1.2.1.2 Theoretical Determination of the Torque

The direct manipulations have illustrated the mechanisms of action for many biological machines and structures that compose each living cell. Although optical force is not the only parameter of importance. Definitely, for a host cell machinery, rotation and torque may be even more considerable The ability to measure instantaneous torque is of great importance, since it will facilitate precise measurement of the torque generated by biological structures as they rotate. In recent years, researchers have developed a variety of techniques and methodologies that enable direct access to these mechanical parameters, allowing for a more comprehensive understanding of the behavior of certain biological components. By combining force, displacement, torque, and rotational data, a more comprehensive description of the mechanics of a biomolecole can be achieved(La Porta and Wang, 2004).

Trapping mirror-symmetric micro objects with a focused Gaussian laser beam produces a rotationally symmetric trap that does not exert torque. There are different ways to set into rotation a micro object inside a trap; i) using a beam with an intrinsic optical

angular momentum (OAM modes) is one of the ways of applying a torque to optically trapped object or ii) by changing the phase relation of two recombined beams split from a single laser beam, iii) breaking the mirror-symmetry of micro-objects results in a net torque even in a symmetric Gaussian beam due to the transfer of optical momentum generated on asymmetrically oriented surfaces(Sacconi et al., 2001).

1.2.2 General Study for Single-molecule Manipulation

Single-molecule manipulation techniques like OT or AFM have many common features. Typically, one end of the molecule under study is attached to a surface and another free end is attached to a probe that can be a trapped bead or AFM tip through which force is applied. The importance of the attachments should not be overemphasize. The extension of the molecule is determined from the position of the probe relative to the surface and force is also derived from the deviation of the probe from its equilibrium position. The precision and accuracy of the measurements depend on the performance of the probe, in addition, the environment during experiment can remarkably influence the quality of the results. For instance, temperature, mechanical vibrations, air currents, acoustic and electrical noise are the environmental factors can be effective in single-molecule manipulation measurements. OT and AFM techniques offer different methods for position measurement however, they have many common issues for analyzing(Rief et al., 1997).

1.2.3 Technical Requirements

Optical tweezers setup are equipped with trapping laser, sensitive position detectors and dynamic position control to improves force calibration, particularly for very stiff traps, and extends the detection bandwidth of optical trapping measurements and stiffness calculation. The main elements are i) a trapping laser and ii) a high NA microscope objective lens(Ashkin, 1992):

i) Trapping lasers is a single-mode laser beam having a Gaussian intensity distribution and is considered diffraction-limited to achieve the smallest focal spot producing the largest optical gradient. High precision optical trapping measurements require a trapping laser with superior pointing and power stability. Fluctuations in beam pointing alter the position of the optical trap, while power instability result in force variations which both increase the measurement noise. Trapping lasers operating in the near infrared (800–1100 nm) wavelength, minimize optically induced harm in biological samples. For most

biological applications the trapping laser of choice is a diode pumped neodymium yttrium aluminum garnet (Nd:YAG) with a wavelength of 1064 nm. These lasers display exceptional power and pointing stability and are available with output powers in excess of 10 W. Single-mode diode lasers and high power near-infrared fiber lasers have also been used for optical trapping(De Silvestri et al., 1990).

ii) The high NA objective used to focus the laser is the second most important component of the optical trapping instrument. The NA of the trapping objective should be at least 1.2 to achieve the sharp focus needed to create a stable trap. This NA can be achieved using a water or oil immersion objective. However, oil immersion objectives offer the highest NA, introduce spherical aberrations that degrade optical trap performance Spherical aberration caused by the mismatch of refractive indices in the optical path. Water immersion objectives are optimal for observing living cells in aqueous media as the refractive indices of the immersion medium and the sample are a closer match than for example immersion oil. The other factor to consider in the choice of microscope objective is the optical transmission characteristics at the trapping wavelength(Neuman and Block, 2004).

1.2.4 Biological Applications

The versatility of optical tweezers technique allows a wide range of measurements. One of these capabilities is the three-dimensional manipulation to “touch” a fixed object with a trapped bead and to measure the object stiffness by measuring the force vs displacement resulting from the interaction.

For cell mechanical studies, a spherical dielectric bead is trapped which acts as handle to manipulate cells. Optical trap is characterized by the trap stiffness (k) and obeys Hooke’s law for small displacements (harmonic potential). Force which can be applied on the cell is then measured by the bead displacement (x) from the trap center. The displacement of the bead can be recorded using video-based position detection or a quadrant photodiode. OT forces are in the range from 1 to 200 pN and trap stiffness is in the range 0.001–1 pN/nm(Neuman et al., 2007).

Among the various properties of cell mechanics, visco-elasticity has been the most widely investigated using OT with varying experimental arrangements like, membrane tether pulling, cell stretching and indentation. The technique has progressed with time, from the experimental point of view (setups and procedures), and with more suitable and stable algorithm for analyzing the data. This has contributed to broaden the range of

OT applications and to improve sensitivity in the mechano-biology field, providing complementary data to those obtainable with different measurement techniques, in particular by AFM. Therefore axial (vertical) optical traps are introduced with similar protocol for cell probing by indentation as AFM(Costa, 2004).

In the AFM techniques, the forces range from 10 to 10^3 pN with a cantilever stiffness larger than 10 pN/nm. However, there are some restrictions that limit its use in small force domain. The thermal noise of the cantilever in a liquid, which is of the order of tens of pN. limits the minimum applied force. Furthermore, as an example, if the stiffness of the cantilever is 100 pN/nm (normally used in biological experiments), any small error in indentation of 1nm will induce a force of 100 pN, which is critical for many of the biological processes. To overcome these limitations, OT can be employed to characterize cell mechanics at small forces (<10 pN). OT, in general, impart forces in the range of 10^{-1} – 10^2 pN with a spring constant of 1-10^3 pN /nm, which makes OT ideal for low mechanical force regimes, and consequently for probing soft materials. The higher sensitivity of OT over AFM lies in the different kinds of probes through which they apply forces. In the case of OT, the probe is a micron size bead held tightly in a laser trap, which is more sensitive than a mechanical cantilever(Deniz et al., 2008).

OT versatility is highlighted by the wide range of applications which this technique has enabled: OT are now being used in the investigation of an increasing number of biochemical and biophysical processes, from the basic mechanical properties of cells to the multitude of molecules and macromolecules that drive the internal biochemical machinery of cells, DNA and proteins, force generation by molecular motors, individual RNA transcription, and protein unfolding/folding or binding/unbinding(Feynman, 2007).

1.3 Motivation and Problem Statement

The main motivation of this work was to set up a method to fabricate by two-photon lithography 3D micro-tools that manipulated by optical tweezers could serve for the characterization bio-mechanical properties of single-cells.

Photopolymerization is a very important class of photochemical reactions used in microfabrication. This is because some resins, based on polymer, oligomer, or monomers undergo significant cross-linking upon UV irradiation, which can be exploited by selective dissolution of the unexposed material in suitable solvents, resulting in well controlled micro-structures after development. Typically, the process is

used in photolithography to produce two-dimensional micro-structures. However, a nanofabrication principle has emerged in recent years based on two-photon absorption. This allows the fabrication of 3D nanostructures. The most synthetic way to explain the reason of this fact is to say that two-photon photopolymerization rate is quadratic in the light intensity. Therefore, by using focused light from fs-lasers, the interaction volume of the light with the resin is a sub-micron scale ellipsoidal voxel centered in the focal spot. This essentially prevents cross-linking of the resin at a different depth in the bulk of the resin film. This principle allows to form three-dimensional structures by scanning the focused laser in 3D(Juodkazis et al., 2009). Two Photon Polymerization has been used for different types of devices, from optical components, to microfluidic devices as well as micro-electromechanical systems (MEMS).

The cell, the basic functional unit of living organisms, maintains and senses the physiological environment within the organism both chemically and physically, from which it receives the cues for differentiating into specific tissues. The unique biochemical and biophysical conditions surrounding a cell induce it to fulfill its specific functions and adapt to its environment. Physiological changes within the cells are accompanied by chemical and physical modifications and reorganization. Biochemical properties of pathological cells have been under intensive study and many biochemical markers have been developed to identify target cells out of a heterogeneous population(El-Ali et al., 2006). The biophysical properties of cells also play important roles in various biological processes and are involved in the regulation of gene expression, differentiation, migration, and metabolic activities.

1.4 Research aim and Objectives

The first aim of this project is to implement a technique for the fabrication of three-dimensional microstructures. The target is to employ 3D micro-structuring capabilities such as freely movable micro-objects more complex than just spherical beads, that will eventually be manipulated by optical tweezers and used as carriers or tethers of biological entities (lyposomes, cells) for force spectroscopy. For the second part of this project, symmetric irregularities introduced in these micro objects for generating torque due to the imbalance of scattering and gradient forces while symmetrical micro-structure are stable in the optical trap.

1.5 Method Statement

The aim of the first part of the project development of the optical set-up and the strategies for fabricating 3D microstructures, optimization of the lithographic performances and writing the software for controlling a piezo-driver. Two-photon photopolymerization has been performed using a sapphire laser oscillator, with 100 femtoseconds pulsewidth, 80 MHz repetition rate and central wavelength tuned to around 780 nm. High spatial resolution voxels of sub-500 nm lateral and vertical size can be achieved in the near threshold region at low laser power (~ 1 mW average as measured in front of the laser source, corresponding to ~ 125 W peak power) and shorter exposure time (<30 ms). Working at low exposure doses per is important to achieve small size voxels, which can be obtained practically by minimizing the laser power. A XYZ piezo-driven stage used in order to scan the focalized fs laser beam in the volume of a suitable polymer. The conditions for optimal lithographic performance will be achieved by proper choice of writing speed, voxel size, power, sensitivity of the resin, and other process parameters. The minimum feature size of the two-photon polymerization process was investigated by exposing individual voxels at different exposure times (10 ms to 30 ms) and at different power (0.4 mW to 1 mW) and comparison between three different objective lenses (UPLANFL 20x/NA 0.5 , LUCPLFLN 40x/NA 0.60 and UPLFLN 100X (Oil Immersion)/NA 1.3) all from Olympus. The highest lateral resolution of a single voxel was 0.3μm while the axial one was 0.35μm.

After optimizing the lithographic technology, the project has addressed the fabrication of three-dimensional structures with interest in the single-cell biology.

We investigated two different photoresists, Ormocer®s a sol gel that does not contain any solvent in ist formalation and remains a viscous fluid after spin-coating, and SU-8 which after becomes a solid film after solvent evaporation. For some photoresists like Ormocer®, the photopolymerization process can be monitor with the CCD camera, since there is a significant change in the refraction index upon exposure, but for other materials, such as SU-8, where the cross-link is induced by the diffusion of a photoacid in a post-exposure bake step, no appreciable chang of the refractive index of the resin can be detected during the lithographic process. The fact that Ormocer® is liquid and SU-8 is solid leads to different exposure strategies and sample configurations. For single cell biology application, microstructures were prepared by TPL on pre cleaned glass

cover slips of 170µm thickness, coated with 3µm LOR 20B or water-soluble Poly-Vinyl Alcohol (PVA) as a sacrificial layers to allow the release of the structures after micro-structure formation in a 20µm thick layer of SU-8 25 were spin coated on the cover slips.

After establishing the process conditions, 3D microstructure like "cone" or "cone with spiral cavity" were fabricated by two-photon polymerization, released from the has been trapped by OT to measure its stability and stiffness as a function of different laser beam power (200 mW and 400 mW). The position distribution of the trapped "cone" is Gaussian and behaved like harmonic potential which can be used for further force measurement study. Symmetrical cones are stable in traps, while asymmetrical cones are unstable in OT and propelled upward in the trap due to radiation pressure. The rotation speed and of the object increase with the power of laser. Also changing the type of asymmetry, different rotation can be introduced. These rotating cones causes micro-turbulence in the surrounding fluid.

1.6 Dissertation Outline

This thesis presents an attempt to study the behavior of micro objects, from mechanical aspects, fabricated by TPL inside the OT trap. It is still challenging to produce complex bio- ompatible micro objects which can be used for analyzing single cell behavior.

Chapter1 discuss four specific points: (a) an introduction describing the background of Two Photon Lithography and Optical tweezers; (b) Motivation and Problem Statement of using these techniques for fabrication of 3D micro structure trapping in Optical Tweezers set-up ; (c) the purpose and aims of the study; (d) a brief explanation of method.

Chapter2 describes the materials and methods used for the development of the lithographic process and the characterization of TPL results and the Calibration of the Optical Trapping and manipulation set-up.

Chapter3 discusses the experimental results in three sections:

Section 3.1 Two-photon microfabrication performance and measures to improve the lithographic resolution.

Section 3.2 Mechanical and optical manipulation of micro-objects, trap calibration, data analysis and explanation.

Section 3.3 Analysis of the rotation and discussion of the torque generated in chiral micro-objects.

Chapter4 conclude all the obtained results and highlight the future perspectives and directions.

2 MATERIALS AND METHODS

2.1 Two-Photon Microfabrication System

This section describes the design and contruction of the experimental setup developed for the two-photon polymerization technique. The setup was built using a fs-laser, common commercial optical elements, a 3-axes piezoelectric stage. The setup was tested with three different objective lenses (UPLANFL 20x/NA 0.5, LUCPLFLN 40x/NA 0.60 and UPLFLN 100X (Oil Immersion)/ NA 1.3). The IR laser beam focused by the microscope objective into a sample, which typically consisted of a 170 μm thick glass coverslip, coated with a sacrificial polymer layer (LOR 20B or PVA) and about 20 μm thick layer of photoresist (SU-8 25 or Ormocer). A software program was written in LabVIEW (National Instrument) environment to convert the discrete points of which a 3D structure is divided into a sequence of triples values that a Digital-to-Analog converter need to provide as triple of voltage values, with a defined clock cycle to control the 3D-scanning motion of the piezo-stage. A CCD camera was introduced to monitor the laser beam spot on the sample, in order to have a mean to adjust its focus and to find the suitable area of the substrate for the writing process.

2.1.1 Laser Specification

The C-FIBER-Femtosecond Fiber Laser by Thorlabs, was used as an IR light source in this project. Its central wavelength is tuned to 780 nm, and delivers pulses of <120 fs duration at a repetition rate of 110 MHz and max average power of ~4 mW (measured at the back focal plane of the microscope objective), power that can be decreased continuously using a variable attenuator.

2.1.2 Optical Setup

Microfabrication by TPP can be performed by scanning a focused fs-laser beam inside the photoresist volume, using for instance a mirror actuated by an acousto-optic modulator or, alternatively, by moving the photoresist-coated sample across the fixed laser beam. In our setup which is described schematically in Figure 2.1, XYZ piezo-stage (NanoMax300-TS, Melles Griot) has been used to scan the sample in the x, y and z directions with the fixed beam. The stage is driven by two controllers (NanoMAX , Two Axis - Melles Griot 17BSC002) connected to a computer via USB ports. The internal actuators are built

directly into the base and provide 20 µm travel range in the three orthogonal directions. The resolution of the piezo-stage is 5 nm, ensured by the feedback from a strain gauge sensors. The exposure time can be controlled through a computer-driven mechanical shutter (Optical Beam Shutter, Ø1/2" Aperture, Thorlabs). The beam is expanded and collimated by a telescope consisting of a bi-convex and a plano-convex lens. After the telescope, the laser beam diameter is 6-7 mm, in order to obtain overfilling of the focusing microscope objective. The laser beam is reflected by a 45° dichroic mirror (DM, red reflector, Thorlabs) directly onto the objective back aperture. The dichroic mirror reflects most of the NIR laser beam and transmits part of the visible spectrum (400 – 550 nm) enabling real-time monitoring of the sample surface with a CCD camera. The smallest spot size of the laser beam is achieved with oil Immersion objective lens (UPLFLN 100X , NA 1.3, Olympus).

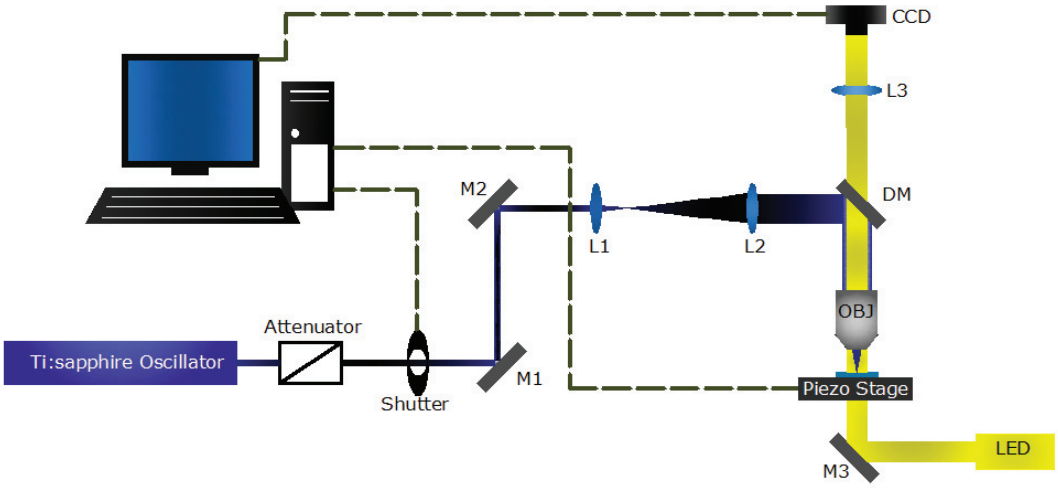

Fig. 2.1 TPP experimental setup; L1 and L2 lenses for beam expander, L3 imaging tube lens, DM – Dichroic Mirror, OBJ – microscope objective

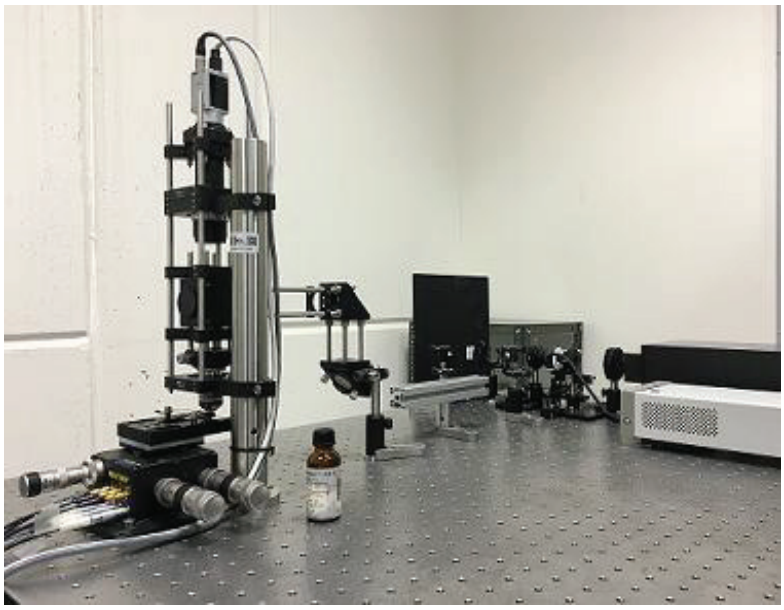

Fig. 2.2 Experimental setup consisting of a Femtosecond (fs) laser, a XYZ piezo-driven stage for 3D scannig the sample, beam expander, microscope objective and other optical elements on a frame mounted on a stable anti-vibration optical table.

2.1.3 Software Development and Computer Control

In the first place, 3D microstructures are designed with the help of 3D CAD (computer–aided design) softwares such as Rhinoceros or AutoCAD. The model of the 3D micro-object is discretized into a list of points. Their XYZ coordinates are extracted and sorted in an Excel file with a routine that minimize the length of the path through the list of points, with the aim of reducing the vibration caused by moving stage during the scanning procedure. As a result, a three-column output text file where every line represents the three x, y, and z coordinates of the displacement vector of the piezo-stage.

A second module, a LabVIEW code, was written to communicate with an APT-based controller software via ActiveX technology. APT software is supplied to use on the host controller PC (APT server). APT server consists of ActiveX controls which provides a graphical user interface (GUI) panels and programmable interfaces that can incorporate hardware control easily through their custom client application.

For example in our project, controllers can be connected to a PC via standard USB to control piezo stage in 3 axis. Coupling this with the very user friendly APT software which has been written by controller manufacturer, allows the user to run complex move sequences in a short period of time. In Melles Griot controller, all relevant operating parameters are set automatically for using the extensive ActiveX programming environment in LabVIEW.

In LabVIEW, we built a user interface, a front panel, from which a set of input parameters can be entered, like exposure time and scanning speed along 3 different axis, to control the piezo-stage and fabrication process. The typical distance between coordinate points must be smaller than the focus spot size to ensure an overlap between consecutive exposed voxel needed for the stability of the final structure, and to increase dose uniformity, thus reducing size fluctuations and surface roughness.

Finally, for any 3D structure, coordinates can be loaded from text files that generated previously into the LabVIEW software to move the stage via controllers accordingly. Before exposure, an input parameter is entered for the conversion of the spatial coordinates into triples of voltage values that the digital-to-analog converter DAC applies to the 3 piezoelectric axes of the stage. The conversion units affects essentially the scale at which the drawing is translated into 3D micro-objects.

2.1.4 Photoresists Material

We have examined two different types of negative photoresists; one is a viscous silicon-containing liquid resists, know commercially as Ormocer®s and the other is the organic SU-8 that after spin-coating and pre-exposure bake can be considered, for all our purposes as solid. SU-8 is polymerized via a cationic reaction, which takes place during the post-exposure bake step.

For some resists, including Ormocer®, the photo polymerization process can be monitor with the CCD camera, as the exposure affects appreciably the refraction index. This can have in some cases negative effects as the exposed structures might be slightly distorted as a consequence of the variation of refraction index. In other for other materials, as for SU-8, a very limited change of the refractive index of the resin is caused during the lithographic process, and therefore no disturbance is introduced altering the laser beam focus by the structures written beforehand(Ostendorf and Chichkov, 2006).

The fabrication process required pre- and post-bake steps, which were perfumed in accordance with the protocol provided by the manufacturer, MicroChem. Post-bake needs SU-8 developer and 2-propanol(Ahmed et al., 2002).

Ormocer is an organic-inorganic hybrid polymer containing a highly cross-linkable organic network s well as inorganic components leading to high optical and mechanical performances as well as thermal stability(Lü and Yang, 2009).

The fact that Ormocer® is liquid and SU-8 is solid leads to different exposure strategies and sample configurations as it shows in figure 2.3(Serbin et al., 2004).

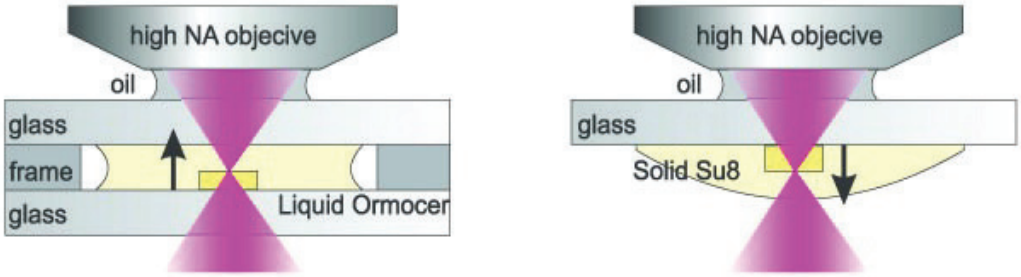

Fig. 2.3 Different sample configuration for solid and liquid photoresists(Serbin et al., 2004)

2.1.5 Sample Preparation

In the prospect of biology experiments on single cells, microstructures were prepared by TPL on pre cleaned glass coverslips of 170 µm thickness, 3µm LOR 20B as a sacrificial layer in lift-off processing and 20µm thick layer of SU-8 25 were spin coated on the coverslips with 2000 rpm spin coating speed for 60 seconds.

In a variant of the previous method, structures at the micrometer scale were fabricated by two-photon lithography in negative SU-8-25 photoresist on a water-soluble Poly-Vinyl Alcohol (PVA) sacrificial layer. 1 µm thick PVA sacrificial layer was spin coated on 170 µm thick glass substrates (microscope cover slips) at 1000 rpm and baked at 90º C for five minutes to remove residuals of water. Furthermore, a step of oxygen-plasma was introduced to improve adhesion between PVA and SU-8. About 20 µm SU-8-25 layer was obtained at 2000 rpm rotational speed for 60 seconds.

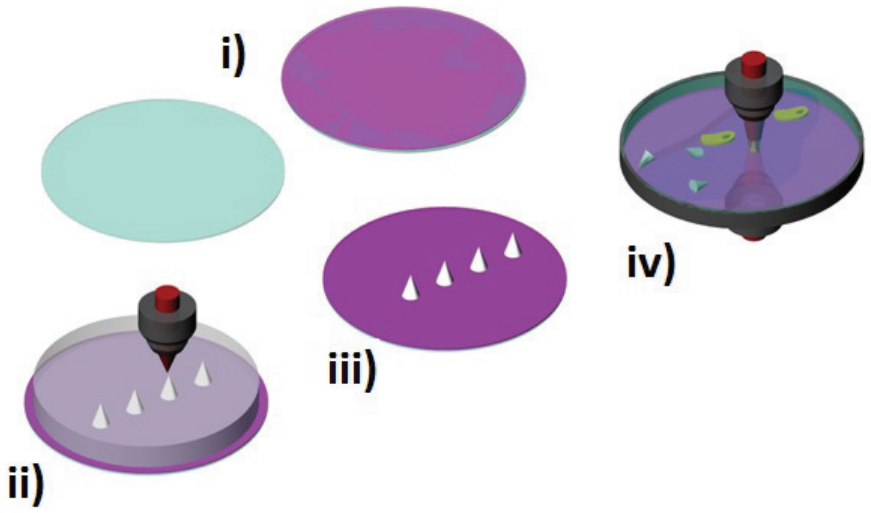

Fig. 2.4 Sample preparation and fabrication process of micro-objects. There are four main steps: i) sacrificial layer spin coating on clean cover glass, ii) SU-8 spin coating on sacrificial layer, iii) exposure and development of photoresist, iv) adding water or physiological solution to release structures from the PVA sacrificial layer and trap them by (OT) set-up

2.1.6 Characterization of the System

As previously mentioned, a major aspect determining the achievable resolution of the lithographic process is related to the properties of the objective lens. This defines the spot size and the depth of focus of the beam. The minimum feature size δ is limited by diffraction and is given by the Rayleigh criterion(Urey, 2004):

$$\delta = k\frac{\lambda}{n * NA} \tag{2.1}$$

where λ is the wavelength (in vacuum), n is the refractive index of the medium between objective lens and photoresists layer (Air (n = 1), Oil (n=1.515), Glycerin (n=1.47) or Water (n=1.33)) (James, 1976)and NA is the numerical aperture of the objective defined as:

$$NA = n * \sin\theta \tag{2.2}$$

NA measures the capacity of an objective to collect light and resolve details of a sample positioned at a fixed distance.

In addition, another important parameter is the depth-of-focus (DOF), which represents the size of the focal spot measured along the direction of the beam propagation (z-axis) and is described by the following equation(Kino and Corle, 1996):

$$DOF = \frac{\lambda\sqrt{n^2 - NA^2}}{(NA)^2} \tag{2.3}$$

In conclusion, the above equation shows that a lens with a longer focal length gives a larger depth of focus. Therefore, the objective lens type and its numerical aperture must be selected according to the application requirements.

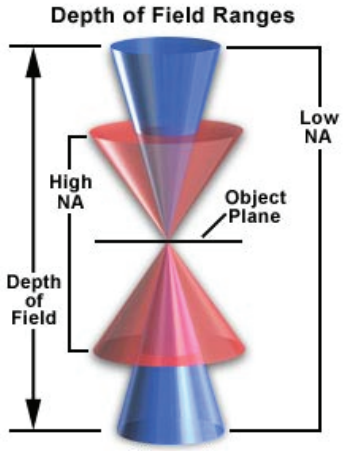

Fig. 2.5 Depth of focus (DoF) is determined by the distance from the nearest object plane in focus to that of the farthest plane simultaneously in focus (Olympus Microscopy Resource Center).

2.2 Optical Trapping and Manipulation

A variety of biophysical methods such as microplates or optical stretchers (Suresh et al., 2005), micropipette aspiration (Discher et al., 1998), magnetic twisting (Planus et al., 2002) , atomic force microscopy (AFM) and optical tweezers (OT) are being used to study viscoelastic nature of cells. However, in the past two decades, AFM and OT emerged as strong candidates to study cells cultured on substrates.

The majority of the optical trapping experiments we performed were done on a plane that is parallel to the microscope coverslip. In this horizontal geometry, it is difficult to compare the quantitative results of optical trapping experiments with AFM indentation experiments because the experimental boundary conditions are very different. Therefore, we adopted a mechanism to probe the elasticity (stiffness) of cells, using the same vertical cell indentation scheme as AFM. This highlights the fact that the cells are sensitive to the applied forces and to the loading rates (measured in N/s) because of their viscoelastic,

inhomogeneous and anisotropic nature and the environment condition affect significantly to the result(Corbin, 2014).

In this project, 3D microstructure fabricated by two-photon polymerization method, trapped by OT set-up to measure its stability and stiffness as a function of different laser beam power. It is essential to analyze the behavior of trapped micro object inside the optical trap, i.e. to calibrate it as a probe, before it can be applied to obtain reliable information on the system been measured in force spectroscopy studies.

2.2.1 Optical Tweezers Vertical Indentation Setup

A modular Thorlabs optical tweezers kit with some modifications has been employed in this work. To achieve more stability and power we replaced the original laser trapping source (single mode laser diode, 975 nm, max 300 mW) with an IR laser (single mode Yb fiber laser YLM-5, 1064 nm, max 5W, IPG Photonics GmbH), as shown in figure 2.6.

The laser head has a built-in collimator providing a TEM00 laser beam with a diameter D=5 mm. After reflection by mirror M1 (the orientation of which can be finely adjusted by screws for alignment) the beam passes through a 2X beam expander, increasing its diameter to slightly overfill the entrance pupil of the microscope lens (Nikon 100X, NA 1.25 oil immersion, WD 0.3).

The beam expander also helps to change the focus of the laser (trap position), which allows to distantiate the focus from the coverslip and to have an additional degree of freedom for adjusting independently the optical focus for imaging the bead during cell-bead interaction as shown in figure 2.7. The laser beam is focused into the sample chamber by the microscope lens, where a 3D micro object is trapped at the point of focus. A home-made temperature controlled holder is connected to the sample chamber (a Petri dish) to keep the cells at the physiological temperature, T= 37° C during the experiments. This is mounted on a nano-piezo stage (Thorlabs, NanoMax 3-axis flexure stage) allowing to control the sample position with 5 nm precision. A second microscope lens (Nikon 10X, NA 0.25, WD 7) collects the laser light scattered by the trapped bead. The scattered light interferes in the back focal plane (BFP) of the second lens. The interference pattern (IP) is imaged by lens L3 (f= 40 mm) onto the quadrant photo detector, QPD, (Thorlabs, PDQ80A, detector size 7.8mm) which senses the lateral and vertical displacement of the trapped 3D micro object, as indicated. When this micro object is in the equilibrium position, the IP is centered on the QPD. A lateral displacement is indicated by an IP lateral displacement, while a vertical displacement is indicated by the change in size of the IP. The lateral and

vertical differential signals (ΔX, ΔY, ΔZ) are obtained combining the signals from the quadrants 1-4 as follows:

$$\Delta X = \left[(1+4)-(2+3)\right]; \Delta Y = \left[(1+2)-(3+4)\right]; \Delta Z = \left[1+2+3+4\right] \tag{2.4}$$

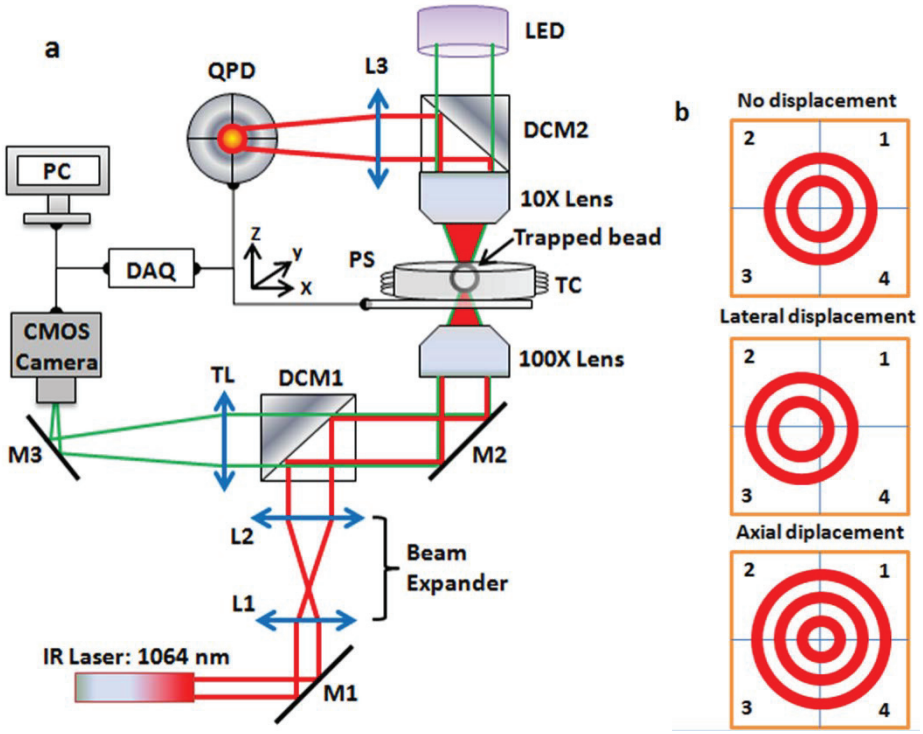

Fig. 2.6 Optical tweezers setup for trapping 3D mico object. (a) Laser trapping beam path (red) and bright-field imaging path (green). PS: 3-axis nano-piezo stage; DAQ: digital analog acquisition card; TL: tube lens; L1-L3 convergent lenses; M1-M3: mirrors; DCM 1-2 dichroic mirrors, TC: temperature controlled holder (b) Interference pattern imaged on the QPD for: equilibrium position, lateral and axial displacements(Yousafzai et al., 2016).

The differential signals are acquired through a digital acquisition card (DAQ – NI USB 2561) and a custom LabVIEW code running on a PC. As the QPD has a large bandwidth (150 kHz), it can resolve the thermal movement of the bead in the trap very well, which is characterized by a maximum bandwidth of 1-2 kHz. The sample is illuminated by the light from a LED through the second microscope lens. The sample is imaged by the first microscope lens and the tube lens (TL) on the sensor of a CMOS camera on the sensor of a CMOS camera (Thorlabs, DCC 1240C).

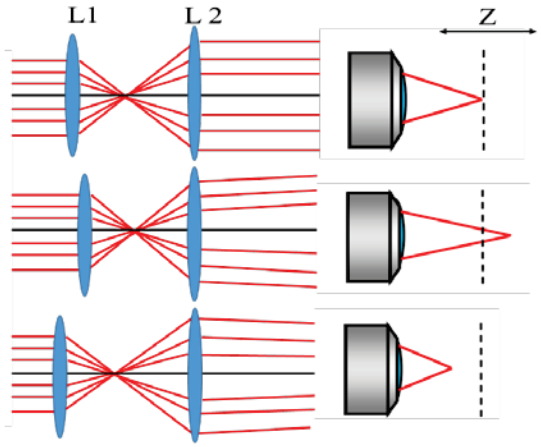

Fig. 2.7 Changing the relative positions of the two lenses of the beam expender, one can increase or decrease the width of the beam as well as the trap location relative to the objective's focal plane (dotted line)(Yousafzai et al., 2016).

2.2.2 Calibration of the Optical Trapping

In order to use optical tweezers as a quantitative instrument for position and force measurements, the detection system must be calibrated. A silica bead of 3µm in diameter was used as a handle for measurements. The calibration of the optical trap stiffness (pN/nm) is based on the measurement of the position fluctuation spectrum resulting from the Brownian motion. The stiffer is the trap (considered as an harmonic potential), the smaller is the amplitude of fluctuations of the bead position. For this purpose a time series position trace of the bead from QPD (measured in voltage units) as shown in figure 2.8. The voltage trace is acquired at 10 KHz for 5 seconds but only a section of 1 sec is shown, which is sufficient to calculate the stiffness.

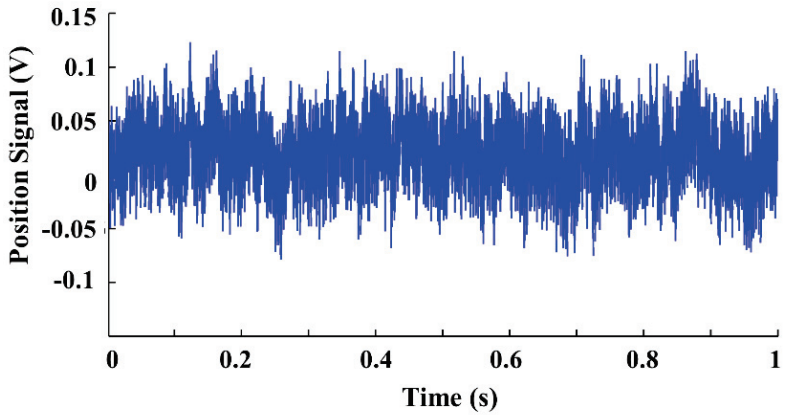

Fig. 2.8 Trace of thermal Brownian motion of a trapped bead from the QPD in volts. The plot is a section (1 sec) of 5 sec trace sampled with 10 kHz.

2.2.3 OT setup sensitivity

To calibrate the QPD signal as a function of the trapped bead position and measure the linear range of the vertical optical trap we focused the trap onto a 3 µm diameter bead that was stuck to the coverslip. The stage is set into oscillatory mode with a sinusoid of 1 µm, in order to sweep the trap position through the stuck bead in the z-direction. The QPD signal in volts vs the stage position in µm is plotted to get the sensitivity of the setup (Figure 2.9). The response was linear for ≈1 µm. From the slope we could obtain the detector sensitivity (0.5 mV/nm), which is necessary to convert voltage trace from QPD to position trace.

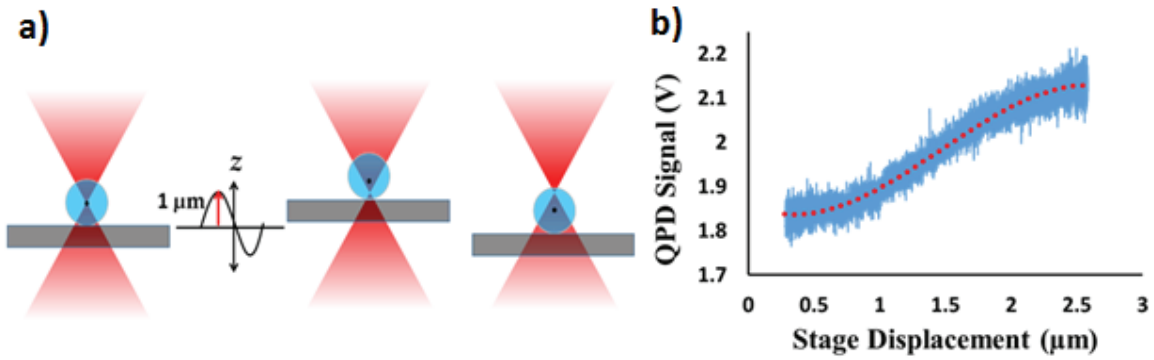

Fig. 2.9 (a) The stage with a stuck bead is moved sinusoidally with a 1µm of amplitude, with trap focus is at the middle of the bead, and the QPD response is monitored. (b) By plotting the linear part of stage displacement and QPD voltage signal we get the QPD sensitivity as V/µm(Yousafzai et al., 2016).

2.2.4 Trap Stiffness Determination

The theorem of equipartition of energy affirm that molecules in thermal equilibrium have the same average energy corresponding to each degree of freedom of their motion which corresponds to(Wang et al., 1997):

$$\langle E \rangle = \frac{1}{2} k_B T \tag{2.5}$$

A trapped micro object in thermal equilibrium moves according to the natural Brownian motion within the potential field generated by the optical trap, around the objective focus. This kind of movements provides useful information about the shape of the trapping potential and represents an effective and elegant scheme for trap calibration. In thermal

equilibrium, the density of 3D micro object position, is established by Boltzmann statistics(Succi, 2001):

$$\rho(x,y) = C\exp(\frac{-U(x,y)}{k_B T}) \tag{2.6}$$

This equation describes a two-dimensional movement and k_B is the Boltzmann constant, T is the absolute temperature, and C is a normalization constant. Qualitatively this equation states that Brownian particles spend more time in regions of lower potential energy. In order to determine the trap potential U(x,y) a simple model based on a few parameter need to be assumed. The optical trap potential is usually modeled as an harmonic potential because the trapping force scales linearly with the micro object position close to the trap center (behaves like simple spring). The density of variable movement of the object inside the optical trap is a particular three dimensional Gaussian (Gaussian Probability Density Functions, figure 2.10).

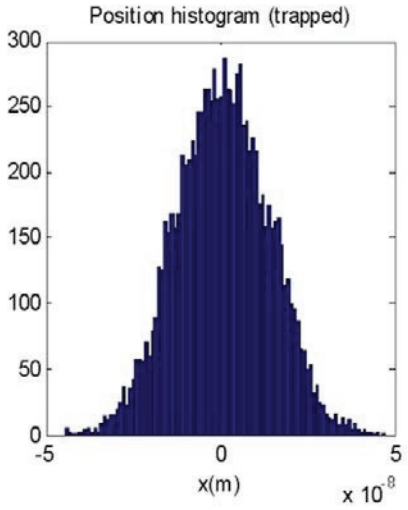

Fig. 2.10 The Gaussian distribution is a general mathematical distribution

$$\rho(x,y) = Ce^{(\frac{-k_x}{2k_B T}(x-x_0)^2} e^{(\frac{-k_y}{2k_B T}(y-y_0)^2} \tag{2.7}$$

where k_x and k_y, are the trap stiffness's in the axis directions, and (x_0, y_0) is the equilibrium position. Considering that we know the temperature, the width of the Gaussian-shaped histogram is directly related to the trap stiffness:

$$k_x = \frac{k_B T}{\sigma_x^2} \tag{2.8}$$

where σ_x^2 is the time-averaged square of the bead's displacement from the center of the trap (equilibrium position) which can be considered as the variance of the displacements. The variance of the displacements in the vertical direction $\langle \mathbf{z}^2 \rangle$ is calculated by converting a voltage trace to a position trace using sensitivity, K_B is the Boltzmann constant and T is the temperature of the medium. Therefore, the stiffness of the trap is(Graessley, 1982);

$$k = \frac{k_B T}{\langle z^2 \rangle} \tag{2.9}$$

This relation is applicable to calculate the estimate the trap potential. However, the results are not very accurate far from the center of laser beam, given that the harmonic approximation for modeling the potential may become invalid(Svoboda and Block, 1994).

2.2.5 Optical Rotation and Torque

For the last part of this project, a new method for rotating asymmetric micro-object inside of single laser beam was examined. The 3D micro-objects with broken mirror-symmetry were fabricated by TPL and trapped by OT set-up. The latter consisted of an IR laser (single mode Yb fiber laser YLM-5, 1064 nm, max 5 W, IPG Photonics GmbH) that is focused into the sample chamber through Nikon 100X lens (NA 1.25 oil immersion, WD 0.3) to produce a stable trap of 1 μm width. The trapped sample is imaged through CMOS camera (Thorlabs- DCC1240C).

3 RESULTS AND DISCUSSION

3.1 Two-Photon Microfabrication Performance

Our system is capable of producing high resolution complex 3D structures. The fabrication time for an object contained in a volume 10 x 10 x 10 μm is usually between 1 to 3 minutes, depending on the resolution and the actual volume to be exposed. The photopolymer chosen for fabrication is a commercial UV curing adhesive (SU-8 25, MicroChem) with optimum sensitivity in the 350-400 nm range.

3.1.1 3D lithographic spatial resolution

The spatial resolution of the polymerization process is the minimum size of the volume that can be polymerized in a single pixel exposure (volume pixel or voxel). The lithographic resolution is correlated to the intensity distribution, but it does not coincide with it. In fact other parameters affect the resolution of the lithographic process, such as the resist sensitivity, processing parameter, such as pre-bake and post-bake conditions, temperature and time of development. Nevertheless, the dimension of the spot size gives a first indication of the minimum feature size that can be obtained. The voxel size is defined by the two parameters: long axis or depth direction of the laser beam, which determines the "axial resolution" and short axis or side by side that specifies the "lateral resolution". The resolution depends on the exposure time as well as on the power of the laser beam (considering fixed the other relevant parameters, i.e. pulse duration, repetition rate, diameter and numerical aperture of the focusing lens). In order to be able to achieve the maximum resolution possible one needs to have a quantitative relation between the size of the voxel, and the exposure dose time and laser beam power.

- For Dry Objective lens UPLANFL 20x/NA 0.5:

Spot Size :

$$1.22\frac{780nm}{1*0.5}=1.9\mu m$$

Depth of focus :

$$780\frac{\sqrt{1-(0.5)^2}}{(0.5)^2}=2.7\mu m$$

- For Dry Objective lens LUCPLFLN 40x/NA 0.60:

Spot Size : $$1.22\frac{780nm}{1*0.6}=1.58\mu m$$

Depth of focus : $$780\frac{\sqrt{1-(0.6)^2}}{(0.6)^2\sqrt{}}=1.73\mu m$$

- For UPLFLN 100X (Oil Immersion)/NA 1.3):

Spot Size : $$1.22\frac{780nm}{1.52*1.3}=0.48\mu m$$

Depth of focus : $$780\frac{\sqrt{(1.52)^2-(1.3)^2}}{(1.3)^2}=0.36\mu m$$

However, the above numbers represent the width of the distribution of the light intensity, which is relevant in single-photon exposures, and not the width of the squared intensity, relevant to the two-photon polymerization process. If the Gaussian distribution for **I** is replaced by the distribution $\mathbf{I^2}$, which is also Gaussian, the width of the distribution is narrowed by a factor $\frac{1}{\sqrt{2}}$ in all three dimensions(Rumi and Perry, 2010). Therefore, the lateral and vertical resolution of the two-photon polymerization process, taking for instance the last objective, would be 340 and 255 nm, respectively. Fabrication of 3D structures was performed from the border of sacrificial layer-photoresist to the surface, starting the cross-linking process from the substrate (i.e. starting from anchoring the structure to the substrate) and moving to the bulk of the resin as it mentioned in Method part.

An important practical aspect of direct laser fabrication is accurate positioning of the laser focal point. If the starting point of scanning is into the bulk of resin but not between the border of glass substrate and sacrificial layer, after development, the structures are lost in the developer, whereas if the laser focal point was in the substrate, some part of the structure is cropped at the base, depending on how deep the focal point was from the interface between sacrificial layer and resist.

To estimate the position of focus point of the laser experimentally, we fabricated a row of voxels polymerized at the same power condition but with different focusing height levels in z direction as shown below. In each step we add +1 µm in the z position from a reference point. After developing we achieved the position for starting point is the reference point +5 µm.

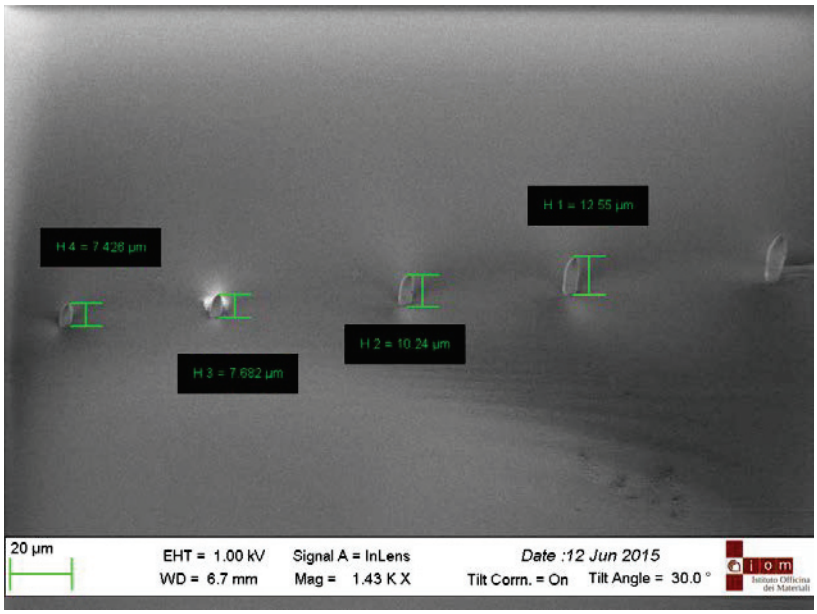

Fig. 3.1 SEM image of a row of voxels polymerized at the same power condition but with different focusing height levels.

Our reference under the CCD camera to adjust the laser point visually was the smallest laser point and the intensity was in the highest level as it shown in figure 3.2.

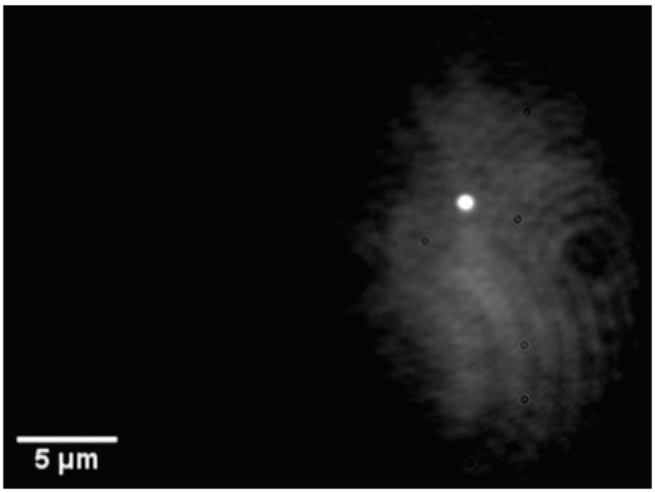

Fig. 3.2 Adjusted laser focus point with the highest intensity under CCD camera

In the next step, the lithographic 3D spatial resolution was characterized from the minimum size of the resin spot or line that could be polymerized on the surface of a substrate. We decided to fabricate a 3D Helix to examine the best thickness resolution and stability on the surface after developing SU-8 to observe our limitation for further steps as shown in figure 3.3.

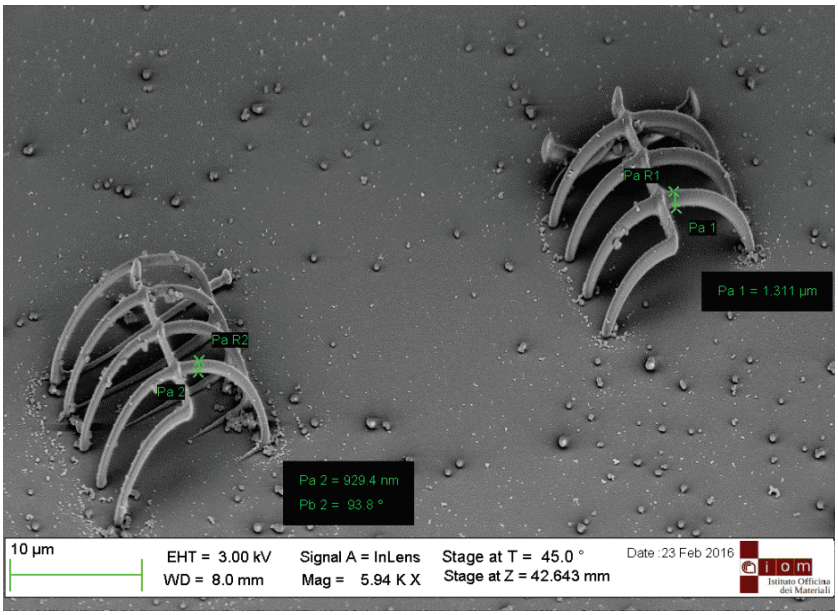

Fig. 3.3 SEM image for 3D Helix fabricated by two photon lithography at 400 µw for two different exposure times (5ms, 10 ms, left and right, respectively).

In figure 3.3, there are two Helixes which were fabricated at 400 µw power in 5 and 10 ms exposure time per voxel. At lower power, both adhesion to the surface and the stability of the structures were too poor as shown by the results reported in figures 3.4, 3.5 and 3.6.

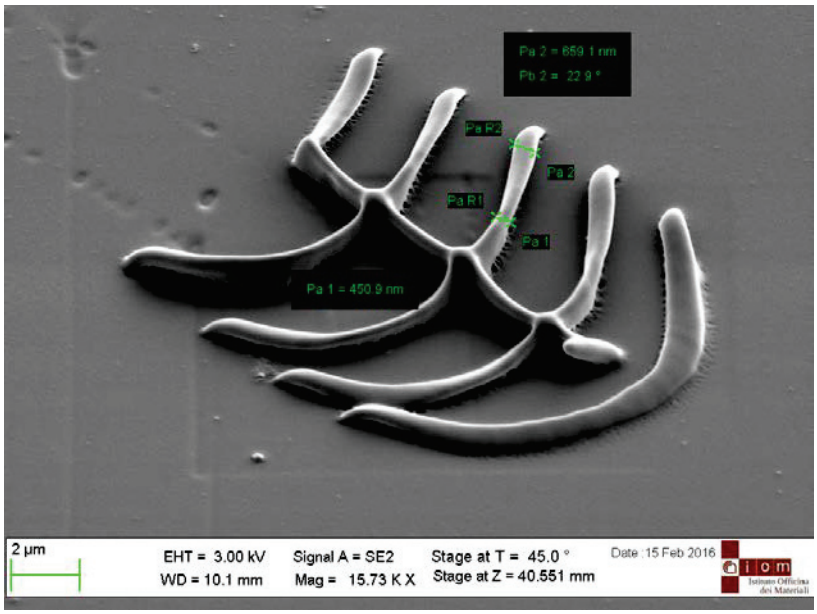

Fig. 3.4 SEM image for 3D Helix fabricated by two photon lithography at 300 µw and 5 ms exposure time.

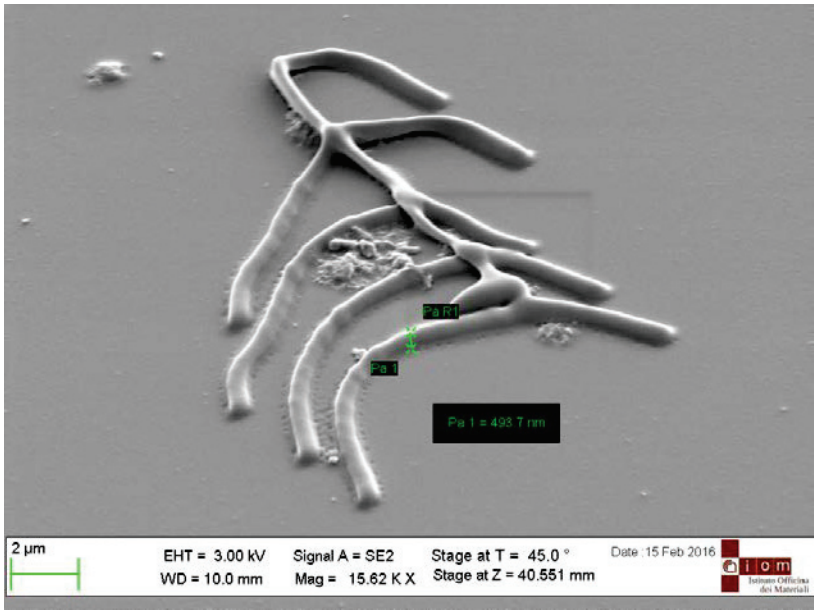

Fig. 3.5 SEM image for 3D Helix fabricated by two photon lithography at 300 µw and 3 ms exposure time.

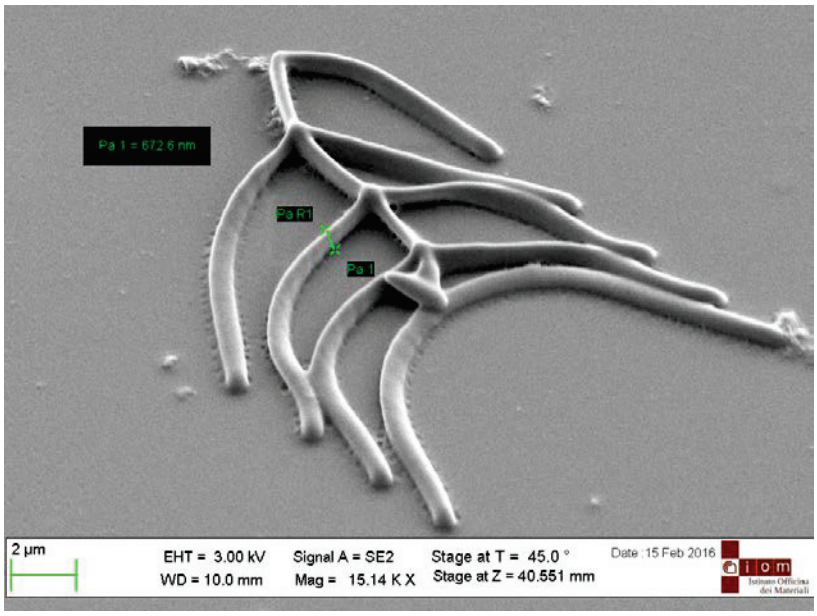

Fig. 3.6 SEM image for 3D Helix fabricated by two photon lithography at 250 µw and 5 ms exposure time.

Therefore, the highest resolution that could be obtained is in the sub-500 nm range, but in order to obtain stable structures (such as suspended lines) the minimum power and exposure time are were 400 µW and 5 ms, respectively. At these conditions, the lithographic vertical resolution was ~900 nm while at the same power and 10 ms exposure time the minimum feature size, measured in the vertical direction was 1.3 µm.

3.1.2 Fabrication and Optimization of Asymmetrical Object

To start with a simple case the study of the trapping of 3D microstructures other than spherical beads (obtainable with simpler means and already object of many publications), we decided to fabricate simple micro-cones. This structure, was taken as benchmark in order to understand how they could be manipulated and whether different issues would emerge compared to the case of spherical beads(Isojima et al., 2009). On the other hand, characterizing the displacement of cones inside of the trap is easier than symmetric object such as spherical, looking at the motion of its apex and base(Guck et al., 2001).

For this purpose we have used a procedure developed for designing any arbitrary 3D structure, starting from a 3D CAD model, which allows to extract and to sort the coordinates of the points, so as to keep minimal the length of the piezo-stage motion, and thus the induced vibration, for obtaining precise structure with smooth surface.

In a set of experiments made for determining a suitable step for the motion of the piezo-stage, we found that the best results are obtained when the exposures are done with a

significant overlap between consecutive voxels. This is necessary to ensure that the exposed micro-objects retain a negligible residual surface roughness. With steps of 500 nm or more, the trace of the individual exposed voxels was clearly distinguishable in the final objects. As shown in Figure 3.7, if the steps size were bigger than the spot size of laser beam, the resolution decreased significantly according to the number of steps. Therefore, the step size was set between 100 and 300 nm.

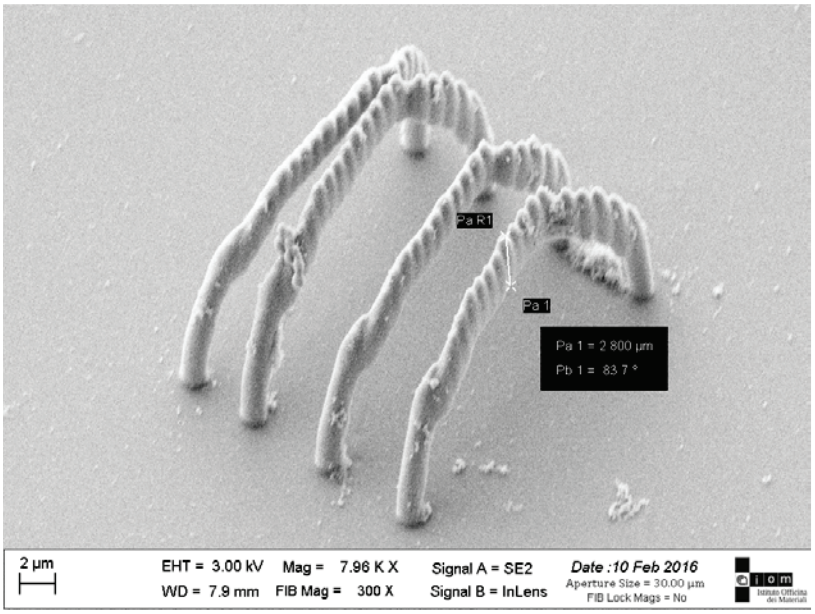

Fig. 3.7 SEM image for 3D Helix fabricated by two photon lithography at 600 µw and 20 ms expo with 1µm step size.

There is another parameter playing a role in the stage motion, which is related to the minimum step in the voltage that the Digital-to-Analog Converter (DAC) can be applied to the piezo drivers. Clearly, the resolution in the stage positioning is related to the resolution of the DAC in setting the voltage applied to the piezos.

We considered therefore that the minimum step in the voltage correspond to a step in the stage of 50 nm. Given that the full travel range of the piezo-stage is 20 µm (in X, Y, and Z), and that this is covered in the voltage range from 0 to 75 Volt, for 50 nm step, the required voltage step to input in the LabVIEW program was 0.1875 Volt.

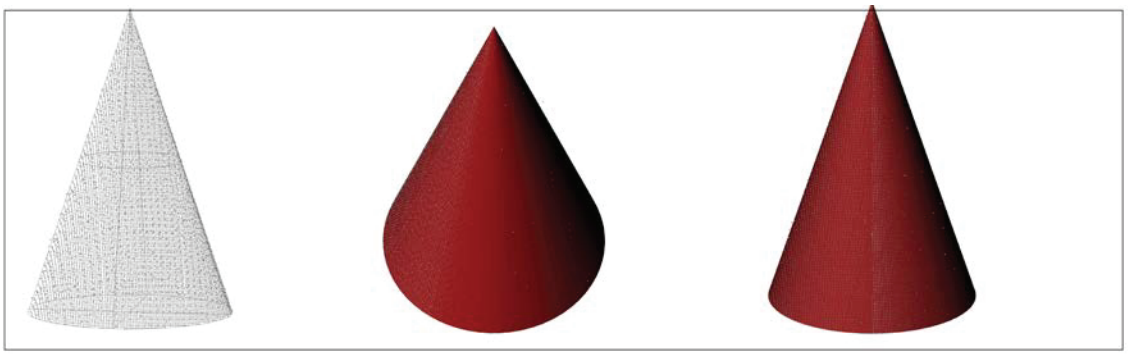

Fig. 3.8 Designed simple Cone in Rhino 4.

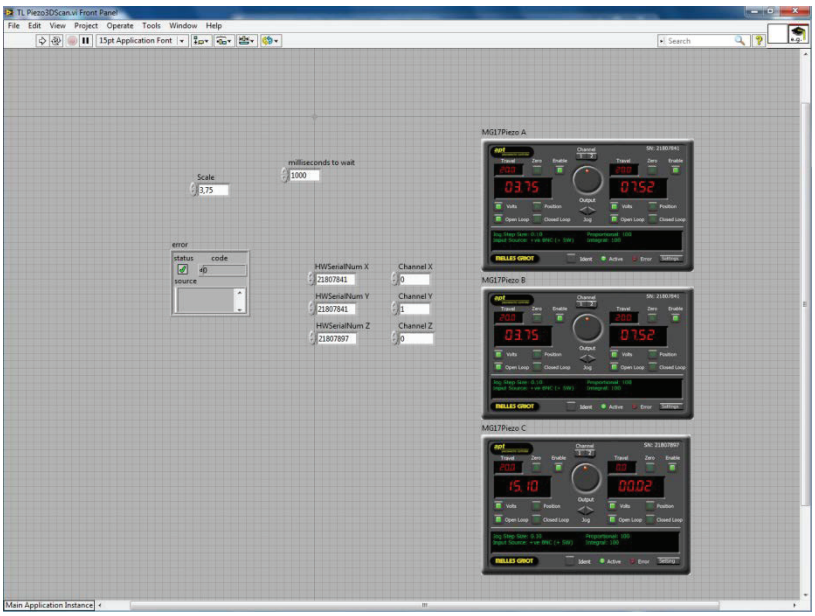

Fig. 3.9 Front Panel of the LabVIEW software, Activex Interface

In Block diagram , each axis from each channel of specific controller, on the associated stage directions, has settings for the Zero Offset and the position is measured from the home position in millimeters. The step and exposure time in each step can be set for the stage axis. The absolute position count is then reset to zero to provide the reference point for all subsequent absolute moves. If position is lost on a stage axis, it should be reset and start again from home position.

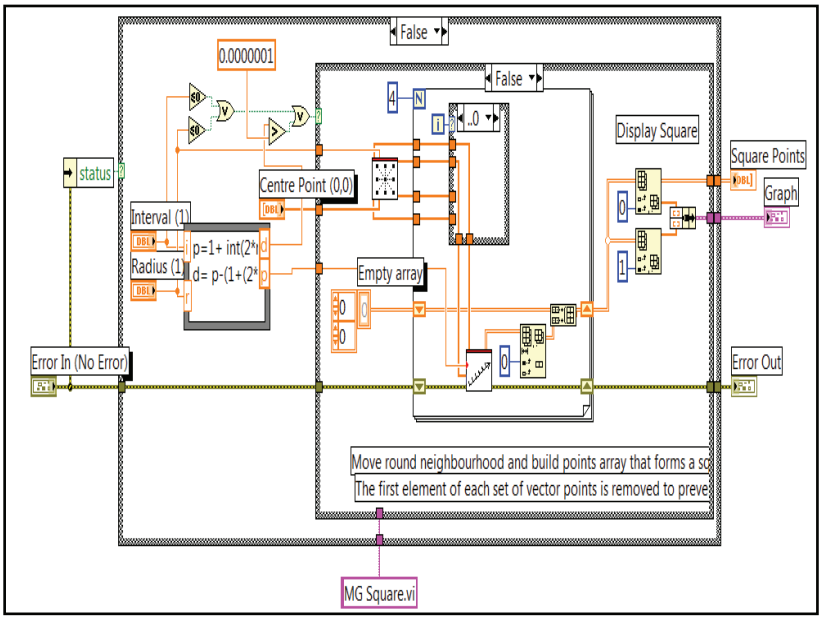

Fig. 3.10 Back diagram of the LabVIEW software, Activex Interface

3.1.2.1 Cone-Shaped Objects

SEM images from the simple cones were acquired, after deposition of a thin metal layer (in general 10 nm sputtered gold, silver or chrome) on the glass substrate to avoid the charging of the surface by the electron beam, which distorts significantly the images reducing the resolution of the images(Goldstein et al., 2012). However, the coating makes the structures not usable anymore for manipulation by optical tweezers. After observing the best condition and optimizing the exposure parameters, the simple symmetric cones are directly released from the Poly Vinyl Alcohol (PVA) sacrificial film, by its dissolution in water, under CCD camera and trapped using the OT setup. The height of these simple cones is about 10 µm and the diameter of their base between 5 to 6 µm.

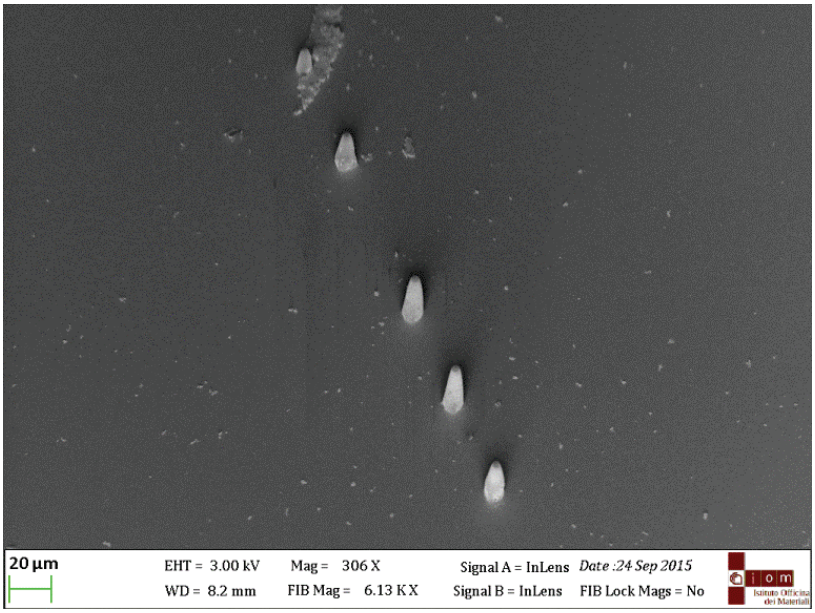

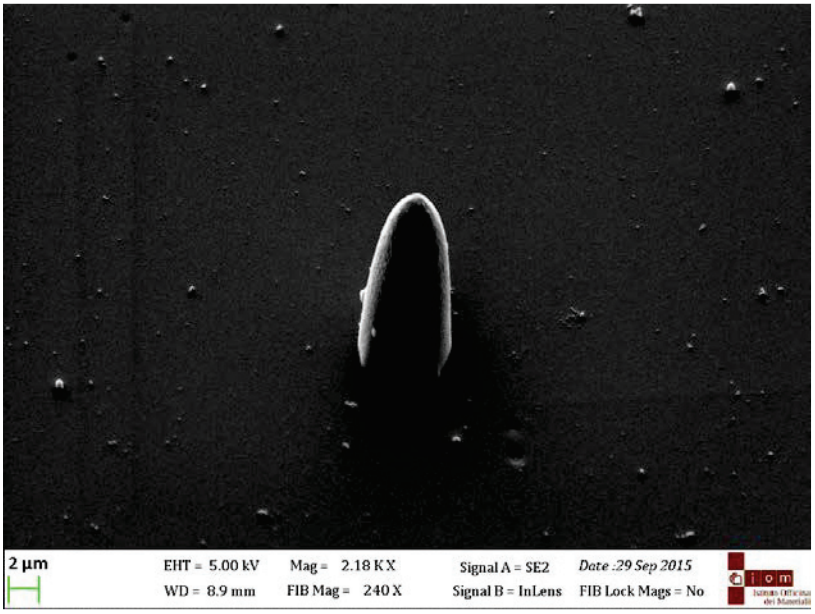

Fig. 3.11 A row of cone-shaped objects for optical trapping

3.1.2.2 3D Micro-structures with Hollow Channels

As we discussed in introduction part, to set a trapped particle in rotational motion, a optically-induced torque acting on the particle has to be generated inside the optical trap. This can be obtained either acting on the side of the laser beam (e.g. using OAM optical modes, carrying an orbital angular momentum), or on the side of the object, breaking the mirror-symmetry. The flexibility of the TPP process allows to control rather well the shapes; thus in the second part of this study, we fabricated cones of the same dimensions

but introducing different features breaking the chiral symmetry. Depending on the magnitude of the symmetry-violation we are expecting a different rotational motion under the same experimental conditions.

To optimize the procedure, different types of 3d microstructures were fabricated, some of which are shown in figures 3.12 and 3.13. As test structures we decided to add to the micro-cones or other micro-objects, grooves along a spiral curve on their surfaces.

As target depth for the grooves we set 1 μm. To achieve this, the the depth of focus of laser beam must be sufficiently small, otherwise the upper and bottom part of the groove on the steep walls of the cone (or of the cylinders tends to merge).

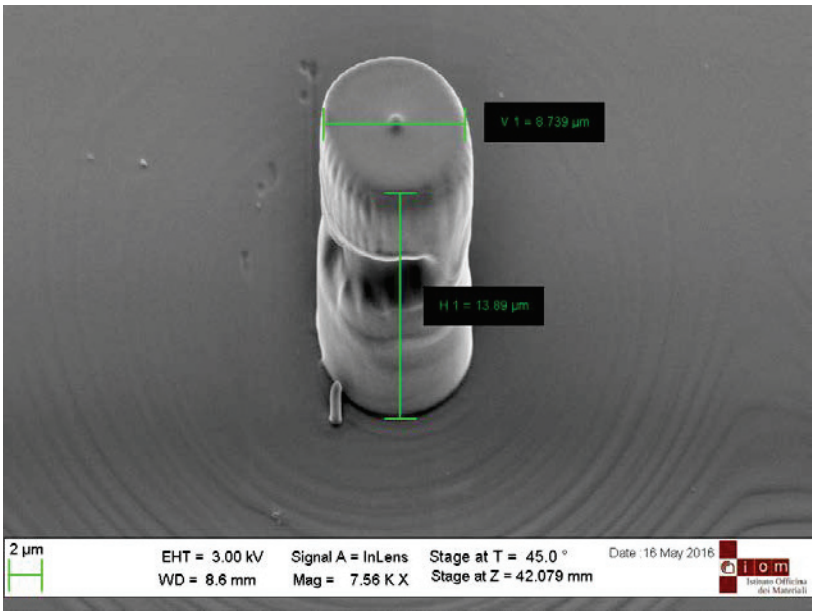

Fig. 3.12 Cylinder with about 2 μm cavity fabricated by TPL

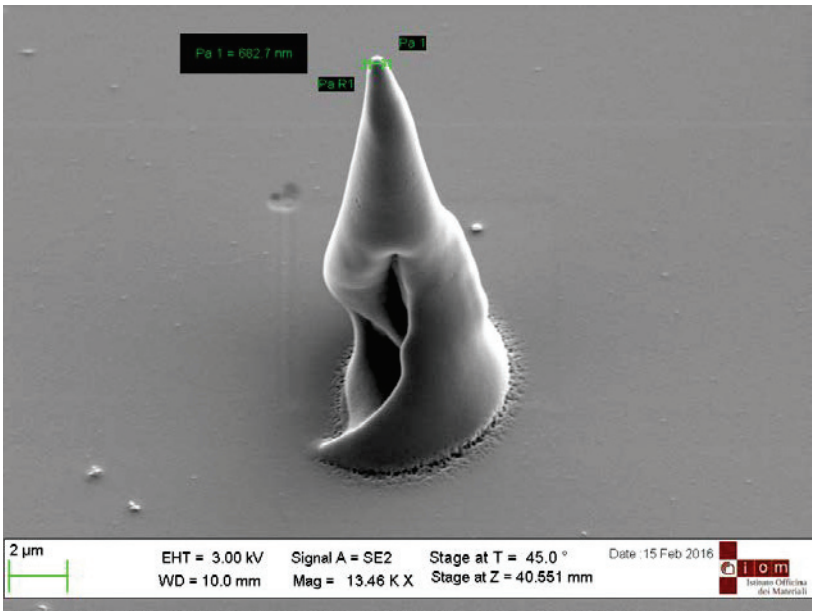

Fig. 3.13 Failed fabrication of cone with deep spiral cavity

Finally, achieving the best resolution allowed to obtain the desired structure to be tested for optical trapping. For further experimental analysis, two different structures were considered, i.e. Type(I) and Type(II) cones. In type(I) the chiral and the angle of spiral cavity is about half of type (II), however the cone dimensions are the same, height of each cone is about 12 µm with 1 µm deep for spiral cavity and the apex radius of curvature is ~ 300 nm.

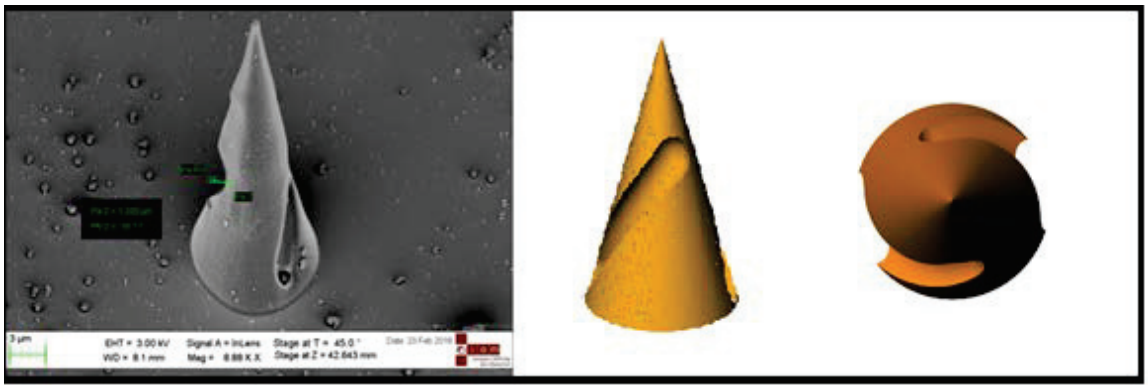

Fig. 3.14 Type (II) : Cone with 45 degree spiral cavity

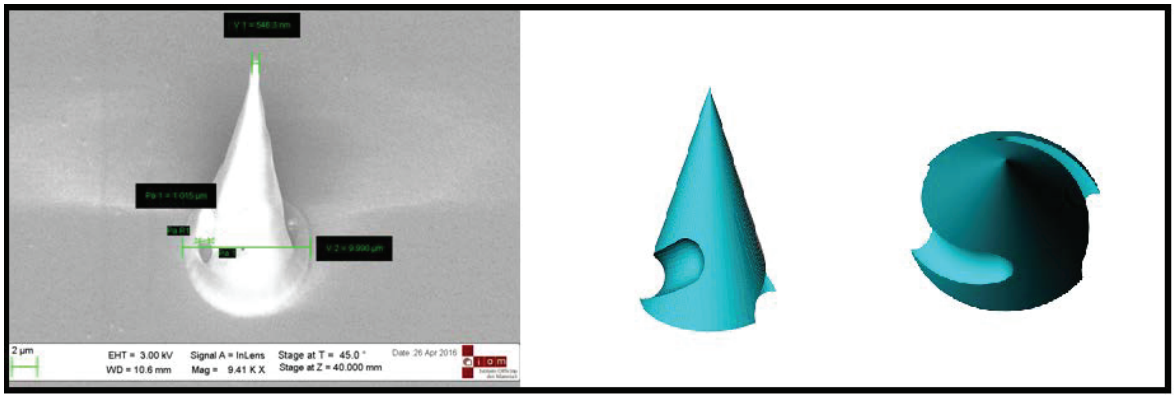

Fig. 3.15 Type (I) : Cone with 22 degree spiral cavity

In the previous chapters, micro objects manipulation by OT setup - simple cone, and chiral cones, type (I) and type (II) were described. Furthermore, the behavior and disposition of these structures inside the optical trap, has been analyzed.

3.2 Mechanical and Optical Manipulation of Micro-objects

For the experiments on optical trapping the glass substrate on which the Micro-objects had been fabricated by two-photon lithography became the bottom lid of a fluidic chamber. The latter is formed taking as a top lid another glass slide, placed parallel at controlled distance from the bottom one with the help of spacers introduced in the gap. Next, this very simple microfluidic chamber is inserted in the OT setup and the gap is filled with physiological solution with the help of capillary forces. This step entails the release of the 3D micro-objects fabricated by TPL in SU-8 by the dissolution of the thin sacrificial layer. This scheme, allows placing a micro-object in close proximity with the OT beam, or already within its optical path before it is released from the substrate. This approach is especially convenient compared to the fabrication of large batches of equal micro-objects, collected with filters afterwards, suspended in solutions, and injected into microfluidic devices, relying on the fact that statistically some of them would reach the place of interest for the experiments. This scheme, here only demonstrated, can be in principle refined, by fabrication of a microfluidic device of higher complexity (with microchannels, fluidic inlets/outlets, reservoirs, etc.) (Verma et al., 2006)in the top lid, and precise alignment of its structures with 3D-micro-objects on a (non toxic, water-soluble) sacrificial layer on the other lid.

Micro-cones and micro-cones modified by added chiral features were chosen as structures for testing the above approach, using OT to demonstrate the trapping and actuation (in this case rotational motion).

3.2.1 Stuck Micro-Object Calibration

The most simple trapping experiment that can be performed by optical tweezers is to trap an object and to transfer to another location while trapped in the focus of a fixed laser beam by moving the fluidic chamber using the microscope stage. The movement of the stage should be made in small steps (usually less than the radius of the object itself) to avoid that the trapped object escapes from the trap due to the drag force exerted on it by the fluid in relative motion with respect to it. In passing, this is also the principle for measuring the maximal force of the optical trap, since by changing the speed of the moving stage, it is possible to determine the speed at which the object is de-trapped. From fluid dynamics laws it is possible to calculate the drag force of the liquid on the micro-object (depending on the size, shape and boundary conditions), which is proportional to the speed(Chaillet and Régnier, 2013). The micro-object is de-trapped when the drag force overcome the trapping force(Dholakia et al., 2008).

In the present case, however, the scope of moving the stage was that of verifying that the object was really trapped by the laser, which could be obtained by moving slowly the stage with manual micrometric screws and not that of measuring the trapping force (which would have required a precise control of the speed, obtainable only with motorized stage. The fine control of the position of the trapping plane requires a calibration.

As already mentioned, the calibration of the optical trap was instead done by studying the Brownian movement of a trapped object measuring the micro-object path accurately. In our laboratory, this is done with back focal plane (BFP) interferometer using a quadrant photodiode detector (QPD) or by video analysis.

3.2.1.1 Voltage Versus Position Calibration

The power spectrum analysis of the position of a trapped bead is usually considered to be the most reliable option. The main idea behind is that the frequency content of the particle motion is related to the strength of the trap. When the stiffness increases, the high frequency components start to dominate the movement of the object(Gomi and Kawato, 1997). Thermally-dependent measurements of the spectrum of position fluctuations give

information about trapping potential, which can be used to calibrate the optical trap(Andel et al., 1996).

The interference pattern that is formed on the QPD fluctuates according to the motion of the micro-object. The different linear combinations of the signals measured simultaneously by the four quadrants allow to extract independently the spectral analysis of the Brownian motion along three orthogonal axes. The QPD detects the displacement from the equilibrium position providing an electronic signal that, for small displacements, is proportional to the x and y coordinates of the trapped bead. Data acquisition from the QPD is carried out with a National Instruments acquisition card (NI-DAQ- NI USB 2561), controlled with LabVIEW.

For this part of the project, simple cone was trapped and the QPD output signal, representing the agitation due to the Brownian motion, was acquired. Figure 3.16 and 3.17 show the plots of measured signal amplitude.

Each cone tracking was acquired for three seconds with a sampling rate of 10 kHz and performed at two different laser powers 200 mW and 400 mW.

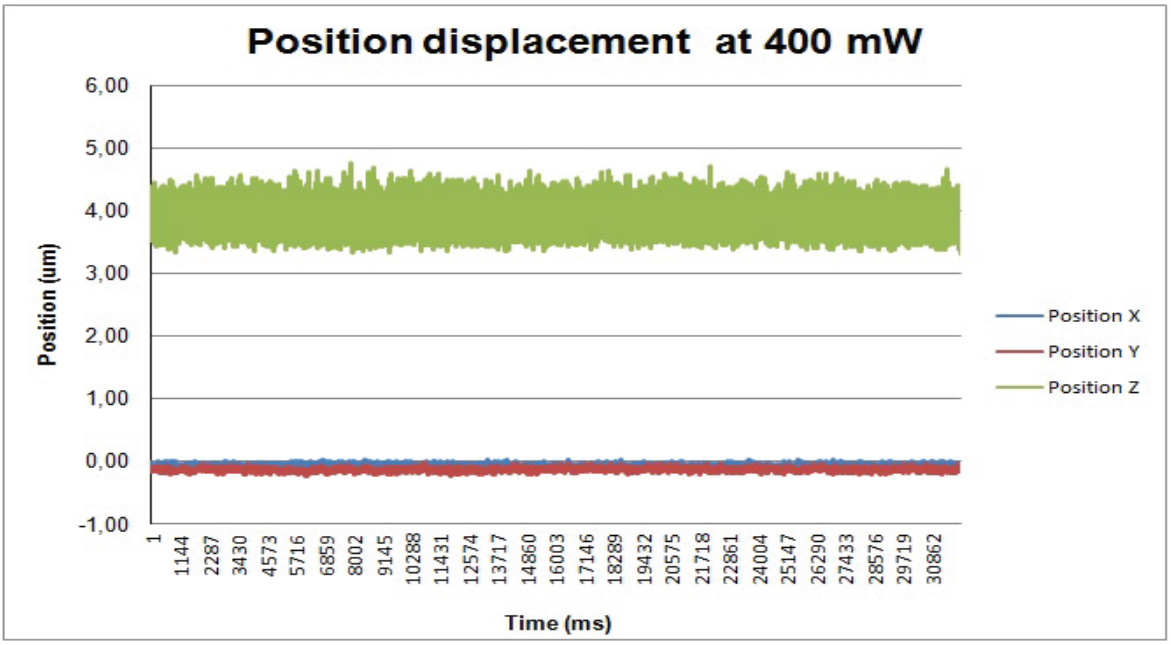

Fig. 3.16 A plot of the position sensitive detector voltage output corresponding to the amplitude of displacement 400 mW, in 3 X,Y and Z axis of a trapped cone relative to the centre of the trap.

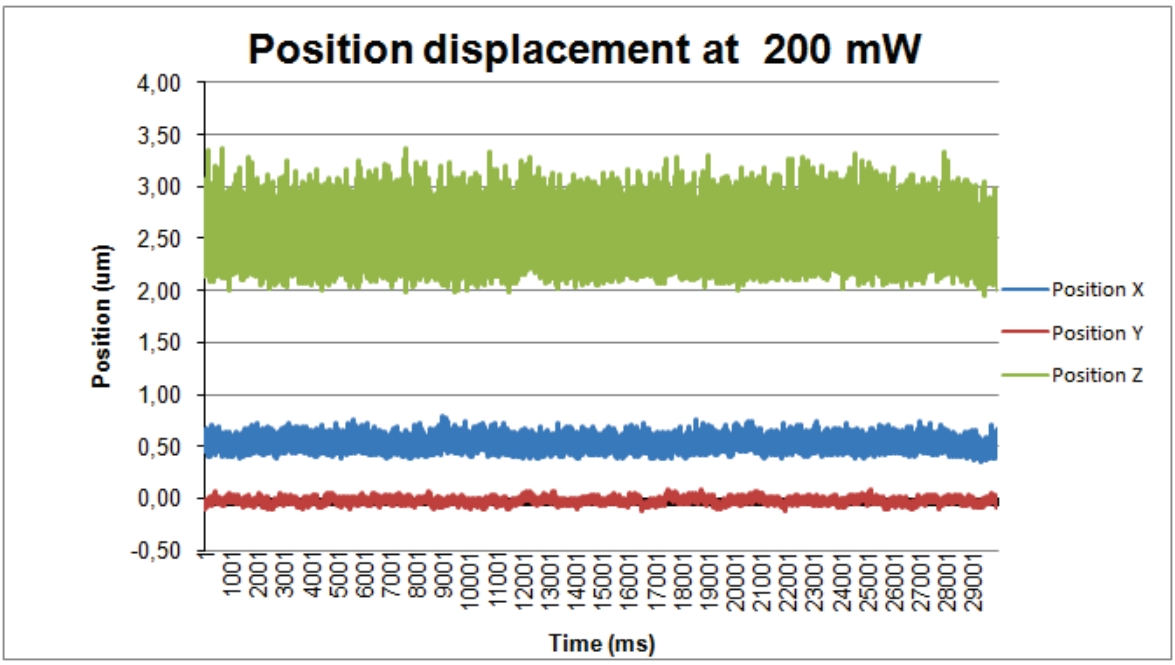

Fig. 3.17 A plot of the position sensitive detector voltage output corresponding to the amplitude of displacement 200 mW, in 3 X,Y and Z axis of a trapped cone relative to the centre of the trap.

As demonstrated above, the behavior of the fabricated cone is substantially the same as that of a spherical bead inside the trap, as explained in chapter 2: by increasing the power, the width of the histogram of the displacement along the 3 different axes decreases, reflecting the fact that the cone is more tightly bound to the equilibrium position of the optical trap.

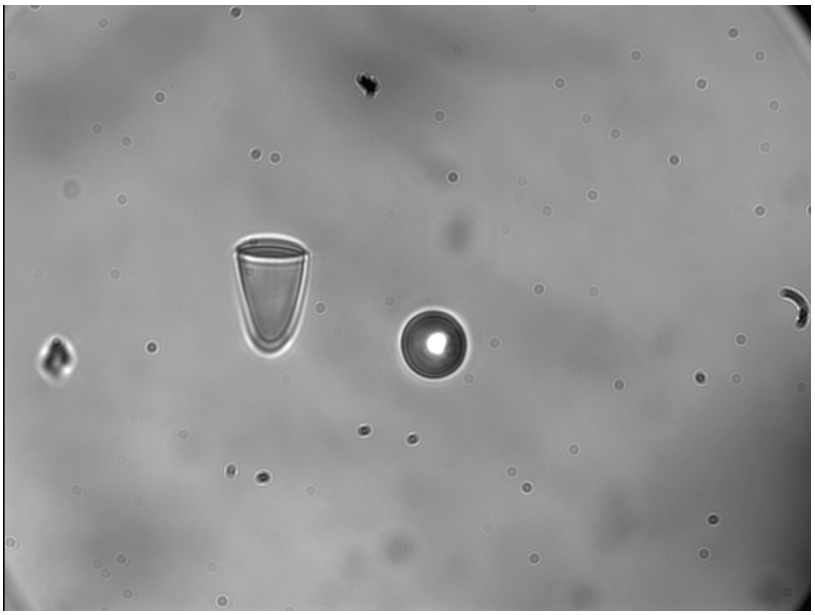

Fig. 3.18 One trapped micro-cone (right) and one free cone (left) imaged by the CCD camera of the microscope. Observe that the symmetry axes of the trapped cone aligns with the propagation direction of the laser beam.

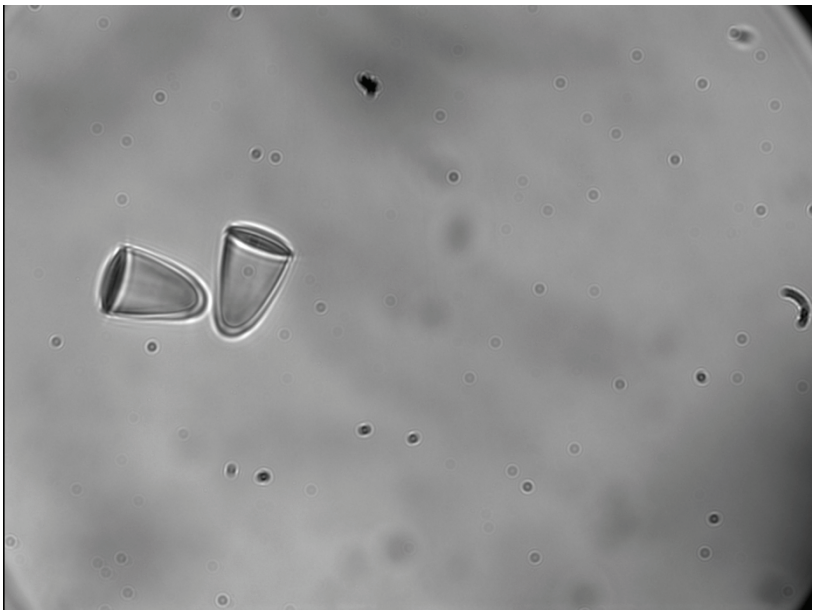

Fig. 3.19 The two previous cones after switching the laser beam off.

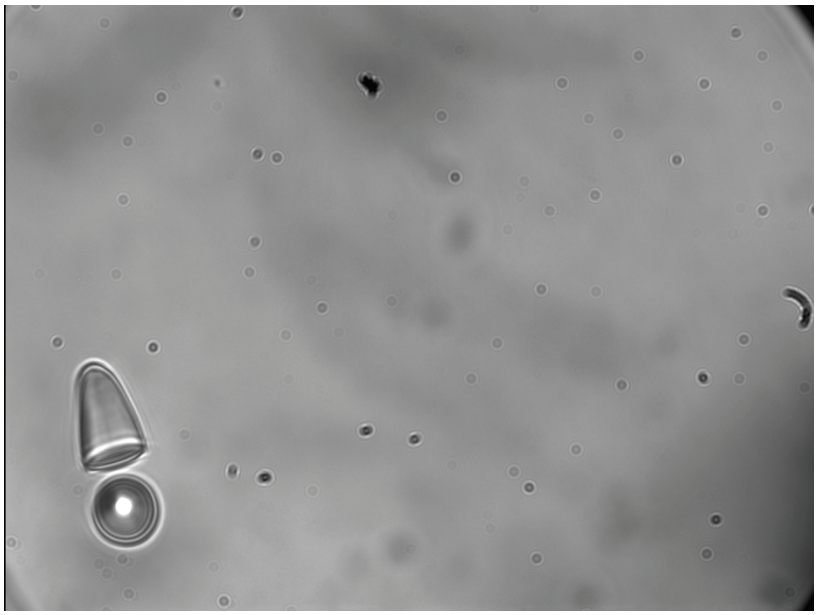

Fig. 3.20 The second cone is trapped, close to the free cone. Again the axes of the cone aligns with the beam propagation direction.

3.2.1.2 Position Distribution Recording

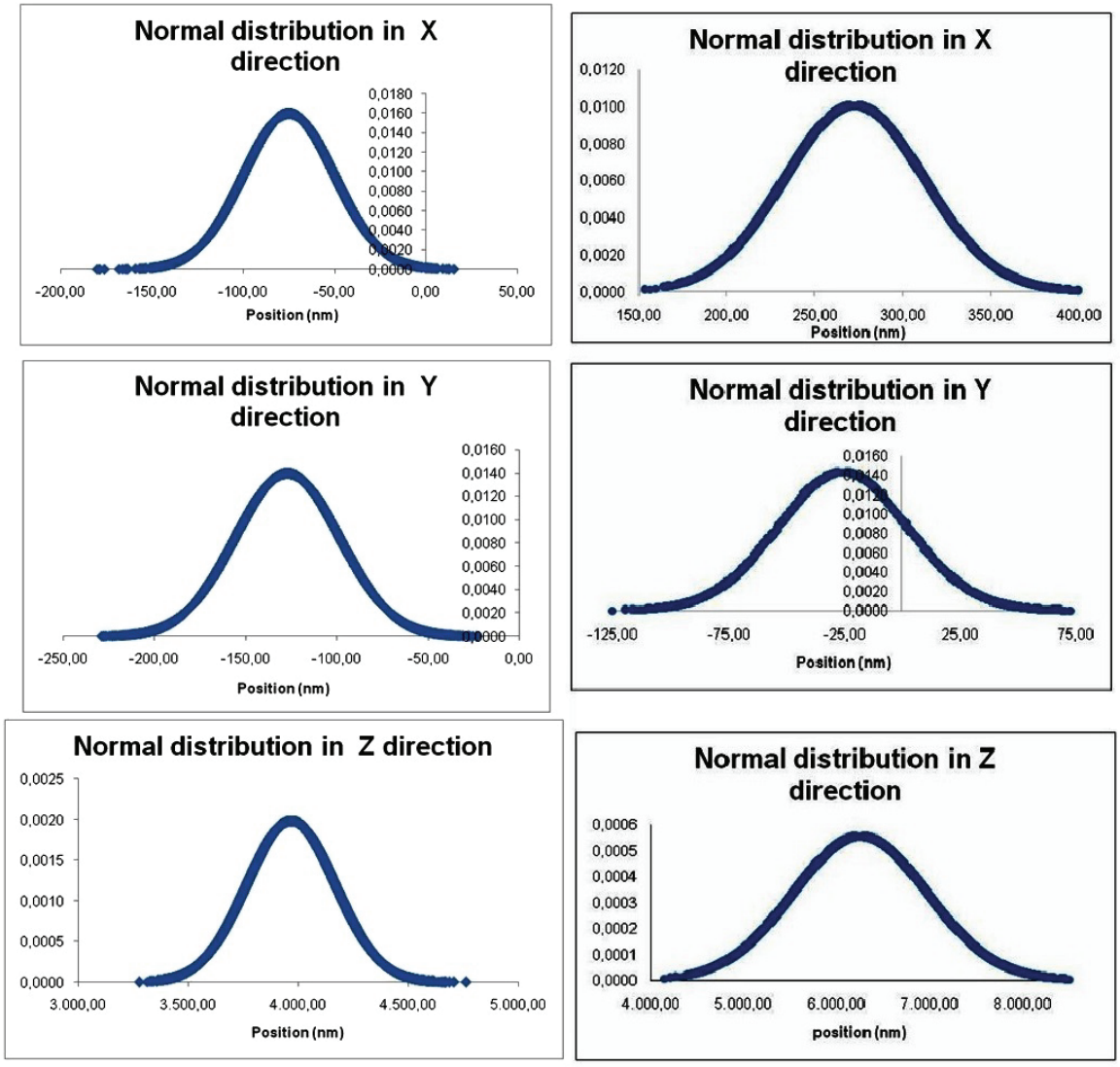

Fig. 3.21 Trapped symmetric cone position histogram in 3 axes (bell-curves)-The right side is at 200 mW power and the left at 400 mW.

Simple cones have momentums and energy that are distributed over a range of values which can be described as a Gaussian distribution.

The results in the z direction followed the same trends as the results in the x and y directions in the calibration methods.

In the classical Boltzmann statistics approach, the trapped cone's position histogram has a normal distribution resulting from a Gaussian trapping laser beam(Yi et al., 2006). Considering the trapped cone displacement we can conclude that our micro structure can be manipulated for further single cell analysis like traditional spherical beads.

3.2.2 Measurement of the trap stiffness

The trap stiffness depends on many factors including the optical power, the diameter of the beam entering the back aperture of the objective lens, the refractive index of the particle and of the surrounding medium, and the distance of the trapped particle from the surface. In order to highlight the wavelength-dependent changes in trap stiffness, changes in the other factors were minimized for trapped particles over the entire wavelength range. However, the fluid viscosity changes dramatically with temperature, and therefore must be determined for each data point.

The second used the equipartition of energy $k = k_B T/\langle x^2 \rangle$, where x is the displacement of the particle from the trap center, and was only linearly dependent on temperature.

The trap stiffness of a simple cone at two different powers at x direction, were the found to be:

At 200 mW :

$$k = \frac{4.11(pN.nm)}{1578,256(nm)^2} = 0.2604\,pN/nm$$

At 400mW:

$$k = \frac{4.11(pN.nm)}{620,79436(nm)^2} = 0.6620\,pN/nm$$

The results in the y direction followed the same trends as the results in the x direction in all calculation for trap stiffness. The results of stiffness calibration method are considered reliable within the trapping laser power range where a linear increase in the trap stiffness with increasing laser power is estimated. While the trap stiffness calculated experimentally in our calibration are in a good agreements with the theory of the stiffness analysis for spherical beads. Typical value has been reported for optical tweezers stiffness is between 0.001 – 1 pN/nm (Malagnino et al., 2002).

3.2.3 Data Analysis and explanation

In the first part of micro-object trapping, a simple cone orient itself along the optical axis with the barb end pointing opposite to the direction of propagation of the trapping laser and was stable inside a Gaussian laser beam trap (fig.22 (a)). These cones obey the harmonic

potential distribution and can be used as handles for force measurements on biological cells with high spatial resolution.

Inside the trap, the cone is constrained by the bottom above the glass slide. This allows to keep trapped the cone in x, y, but independently to move the focus up and down without affecting the position of the cone in the z direction. On the other hand, the cone trapped and has been rotated pivoting on its tip on the glass slide and became stable inside the laser however can be moved in x and y directions by moving the piezo stage.

The rotational speed is corresponding to the z position of the optical trap. At the peak of the cone, is the condition at which the interaction between the optical beam and the micro object is maximal and the maximum rotation happens when the focus of optical beam is close to the centre of cone.

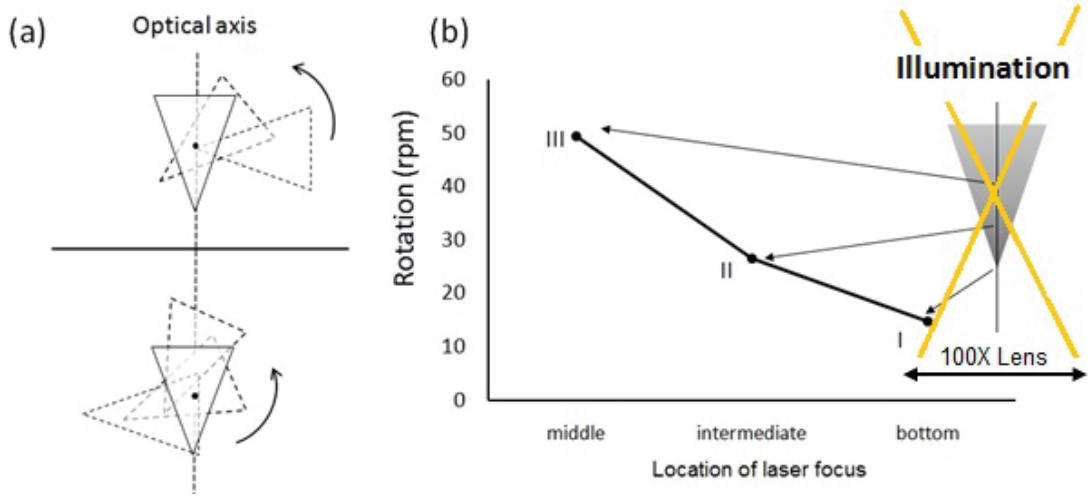

Fig. 3.22 The height of the cone is about 12 µm.
(a) Orientation of the cone in laser trap. The cone's barbed end is always oriented opposite to the direction of propagation of trapping laser. (b) The change in rotation speed with the focus of the trapping laser. The rotation is maximum when the focus lies at the center of the cone (location I).

In this part of the project, the potential for manipulating non-spherical micro-objects has been investigated. We adopted the simple technique for releasing these objects by using biocompatible sacrificial layer for future work on the analysis of mechanical properties of single living cells. Since the strength of the optical trapping depends on the power of the laser beam, one can readily tune the trapping force with variation in the power of the laser beam. On the other hand, two photon lithography fabrication, may enable fruitful applications using arbitrarily shaped objects in MEMS and Lab-on-a-Chip.

3.3 Rotation and the Corresponding Torque Generated by the 3D Micro-Object

With the same trap configuration we could also rotate 3D micro-objects, fabricated by TPL with features intentionally introduced to break the mirror-symmetry. Chiral cones type (I) and type (II) were used and were found unstable in OT and propelled upward in the trap due to the combination of optically induced forces and hydrodynamic forces generated by the rotating object causing micro- turbulence in the surrounding fluid. To achieve 3D trapping we introduced a coverslip to hinder the cone upward motion. In different power, we tracked the chiral cones rotation at 20 frames per second for 30 seconds.

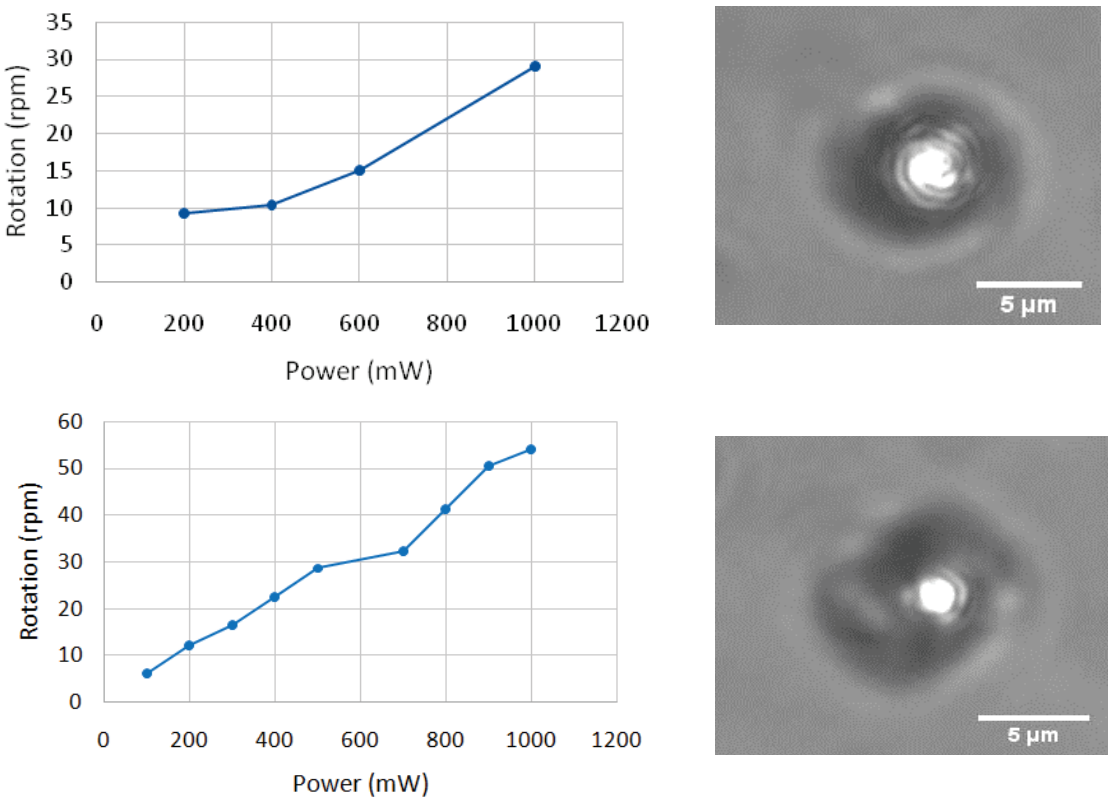

Fig. 3.23 Optically induced rotation of chiral cones. The height of each cone is about 12 µm and the peak is less than 500 nm with 1 µm deep for spiral cavity in water. They rotate clockwise with the laser power between 100 to 1000 mW.

3.3.1 Change of rotation speed with power and type of asymmetry

The rotational speed was almost proportional to the incident laser power and the rotational direction can be chosen by designing an appropriate asymmetric geometry. We trapped two different types of chiral cones with the same dimensions but with different chirality (type I and type II) and their angular rotation differs. The two types show similar behavior for lower power, but as the laser power rises the rotation speed varies differently.

The fabricated chiral cones are not exactly as designed, however they rotated clockwise between 5 to 50 rpm with a laser power of between 10 to 1000 mW.

In conclusion, directional and high-speed rotation were demonstrated for micro fabricated objects having anisotropic geometry but rotational symmetry on the horizontal cross section. This optically induced rotation, on the other hand, requires no mechanical contact and no electric wires, so it can be expected to play a significant role in micro-fluidic device such as remotely driven motors and actuators.

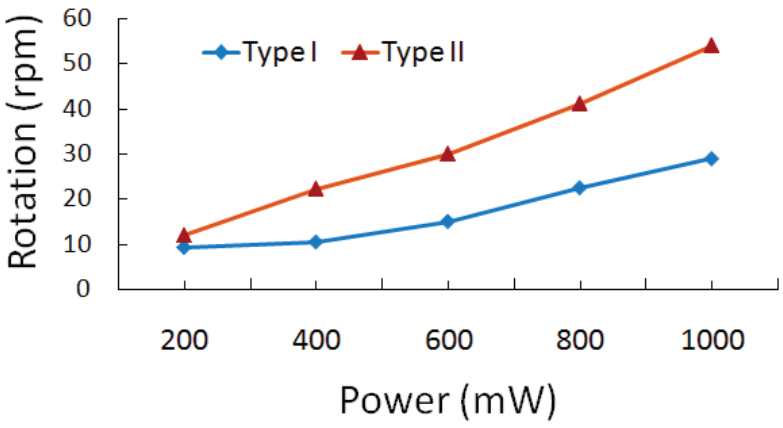

Fig. 3.24 Laser power as well as asymmetry dependence on rotation of cone. Different asymmetries produce different torques and hence the rotation.

3.3.2 Micro propeller and circling objects

In this study, we demonstrate successful manipulation of 3D micro-objects fabricated by TPL not only for a handle or tether for single cell analysis but also for producing rotational motion in the fluid.

When the cone rotates, it rotates the fluid around it and applies a drag on the surrounding micro-objects. Figure 3.25 shows an arbitrary micro-particle, when it enters the revolving fluid region, following a semi-circular path. This micron size cone behaves like mini propeller (motors) creating a local turbulence the fluid. The change of the z-coordinate of the micro-particle of the focus of the circulating object also confirms the continuous circular motion of the fluid.

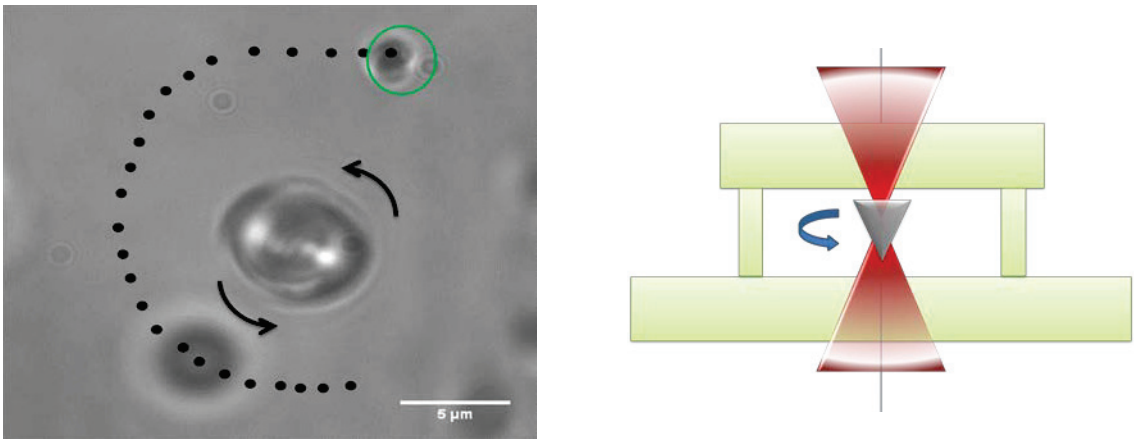

Fig.3.25 The cone rotates in the trap in counterclockwise direction- in this image can be seen two frames after rotating the asymmetric cone . The rotating cone acts like a µ- propeller and circulate the fluid around it (frame one) and the ordinary shaped particle (encircled in green) follow the dotted path during cone rotation(frame two).

A non-contact manipulation method producing local induced rotational fluid flows created by 3D cone has been examined. The chiral cone is rotated in water or other viscous fluid due to the optical forces generated on asymmetrically oriented surfaces to create rotational flows, which act to move micro-objects in the flow region.

This experiment determined manipulation characteristics for the complex flows. Due to its untethered and non-contact operation, this micro-manipulation method could be used to quickly move fragile or non-fragile micro-objects in inaccessible or enclosed spaces such as in lab-on-a-chip devices.

3.4 Discussion

Two Photon Lithography today can be considered as the finest 3D printing technique, with completely structuring capability down to the sub-micrometer scale resolution(Reuss et al., 2005). The low speed of TPL does not allow a widespread use, but in research and for special applications it has the potential to provide valuable solutions to 3D microfabrication issues where no other suitable method is available. A configuration based on a 100 magnification (Oil Immersion / NA 1.3) microscope objective through a glass slide supporting a photoresist film was used to scan the latter within its volume. A CCD camera was used to monitor the focal condition and the XY position of the laser spot. The camera collects the microscope view of the sample surface and projected it to a larger computer screen.

A negative photoresist SU-8 was found appropriate as a material for high-aspect-ratio and three-dimensional (3D) lithographic patterning. A variety of micro-objects have been fabricated using TPP with a spatial resolution of in the submicron range. Simple symmetric cone and chiral conical micro-objects were successfully fabricated using the TPL technique. Two specific parameters in this system were targeted for optimization. 1) step size: which is the distance between points in a pattern, and 2) exposure time, which is the amount of time that the laser is focused at a certain point in the pattern. These values can be used to improve precision and accuracy of the resist patterning with the ultimate goal of using the system for 3D fabrication.

In this project, water was also used for releasing micro structures from the surface and were directly trapped by OT. Water-soluble polymers had two interesting characteristics for our application. 1) They can be deposited conveniently by spin-coating, and the solvent can be removed easily at 190°C for 5 minutes and 2) the resulting layer can be dissolved in

water in room temperature and no corrosive reagents or organic solvents are required. This technique is compatible with our fragile microstructures that might be damaged during typical surface micromachining processes. This approach, not yet in use for biological applications, enabled the direct use of micro-objects from the substrates, eliminating toxic solvent residues, thus proving suitable for cells manipulation.

Optical tweezers has proved to be an extremely powerful tool in the investigation of biophysical processes, for studying for example the activity of motor proteins and other enzymes which biological activity involves converting chemical energy into mechanical work(Vale and Milligan, 2000). The ability to measure displacements with nanometer resolution and to apply piconewton-level forces in a controlled manner makes optical trapping ideal for studying the motion of biological macromolecules. Through the use of optical tweezers it is possible to apply a force, at given positions, at different loading rate, or controlling other mechanical parameters, which can be used to highlight interesting mechano-biological aspects of cells(Au et al., 2016). The possibility of fabricating fine 3D micrometer-scale tools, opens new possibilities of performing complex actions on living cells(Randall et al., 2007).

Under low Reynolds number conditions, the thermal motions of a trapped object, in the present experiments a cone, in solution depend on the trap stiffness(Brouhard et al., 2003). The simplest of all calibration methods is variance-based, and uses the positional variance of a micro object $\langle x^2 \rangle$ in combination with the Equipartition Theorem to compute the stiffness from $\kappa_x = \langle x^2 \rangle / k_B T$, where $k_B T$ is the thermal energy. In the power spectrum method, the frequency-dependent amplitude of positional fluctuations is computed, and data are fitted to the behavior of a thermal particle bound in a harmonic potential, which is a Lorentzian function.

In the optical tweezers setup, by focusing a laser beam through a microscope objective, it has been found that symmetric micro structures are attracted to intense regions in the beam and could be held permanently at a focal point. The position and displacement of a symmetric cone inside a optical trap measured with nanometer precision and the behavior of fabricated micro structure have been studied. Most force-measurement methods treat the optical trap as a harmonic potential well or virtual spring that pulls the bead toward the trap center. A simple cones shows stability in optical trap with their barbed ends pointing against the laser direction. The small surface area of the barbed end can be used as a handle for localized force measurements with high spatial resolution.

We demonstrated the use of a laser trap and back-focal-plane position detector to measure the rotation in aqueous solution of asymmetric cones. The chiral cones fabricated by TPL have different degrees of asymmetry that produce different torques and rotation in their aqueous environment. Type (I) was a cone with spiral cavity inclined at 22 degrees and trench depth of about 1 μm, and type (II) was a cone with spiral cavity inclined at 45 degree and the same trench depth. We presented details of the design, fabrication of 3D micro objects and the testing by a single-beam optical tweezers apparatus of the exerted force, demonstrating the generation of a torque inside the optical trap induced by the chirality of the object. The rotational speed as a function of laser power was measured. The chiral cones, with broken mirror symmetries, shows only 2D trapping and are propelled along the laser direction of propagation. When they are trapped in 3D by introducing a coverslip, to stop the upward movement, they behave like micro-propeller (rotors), creating a local turbulent flow in the surrounding fluid.

These kinds of tiny propellers can find potential applications in microfluidic devices and this method can have a variety of applications ranging from early stage disease diagnosis to quality control in microfabrication.

4 CONCLUSION AND RECOMMENDATIONS FOR FUTURE RESEARCH

The performed experiments prove that the scheme combining the fabrication of 3D micro-tools and their actuation by optical tweezers could become a powerful strategy to construct probes for the manipulation of micrometer-sized objects. In particular, this possibly, may have a particular interest and impact on the study of biological systems, such as cells and tissues. The flexibility of two-photon lithography in creating micro-objects of arbitrary shape may allow designing probes specifically tailored to the mechanical function that they need to realize. The actuation of these probes by optical tweezers will open the way to perform complex actions on living cells with forces in the 1 pN to 1 nN range.

4.1 Summary

This section summarizes the main contributions of this thesis: the demonstration of a scheme of practical realized by two technologies, i.e two-photon polymerization and optical tweezers, in view of their application in biological and biomedical field.

Starting from the second one, optical tweezers, this was developed and calibrated in order to manipulate without contact biological interest particles. BFP interferometry were used and a QPD was added to our setup in order to detect the particle movement in the optical trap. In this method, QPD method permits to perform accurate measurements, enabling the measurement of the stiffness of the optical trap. We studied how the trap stiffness is changing as a function of laser power. The properties of the optical trap compare well with those that were found in literature.

A custom setup for two-photon photopolymerization, was constructed and its performances, in terms of fabrication resolution and experimental results were presented.

We employed two-photon lithography to fabricate micro-objects to be trapped and manipulated it in a biological medium. In particular, cones modified introducing chiral features, were used to show the possibility of actuation in rotational motion. This cones with broken mirror-symmetry, and other micro-objects fabricated by TPP and released in proximity of the system to be studied would allow for instance to acts directly to the cell membrane. A solution for not losing a large number of microstructures during the development process, to transfer in a biological medium and to find it easily, was presented.

4.2 Conclusion

We have demonstrated the feasibility of fully-automated trapping and manipulation of non-spherical micron-sized objects using optical tweezers. Furthermore, the capabilities of rotational asymmetric micro-objects were investigated.

Although we have dealt with only two kinds of shaped objects, these demonstrations, we believe, will open up new possibilities for manipulating arbitrarily shaped objects in addition, will enable exciting applications in cell biology such as the non-contact tools or tethers live cells.

4.3 Future Research

As a future work, we would like to employ the asymmetrical cones in force measurements experiments. To make this method competitive as a force measurements method it will be necessary to optimize the shape of asymmetrical micro-objects, in order to keep them stable in the optical trap while rotating.

Thanks to the intrinsic 3D shaping properties of TPL, different shapes with continuous profiles will be easily achieved for the microstructures.

The application of torque using optical trap is in the early development stage, each individual particle size needs to study comprehensively about control technique and aspect design.

Applying small and controllable mechanical forces on cells, one can study the mechanical signature of the cells that become cancerous contributing to the characterization of important aspects of a disease from the bio-mechanical point of view.

BIBLIOGRAPHY

AHMED, A., BONNER, C. & DESAI, T. A. 2002. Bioadhesive microdevices with multiple reservoirs: a new platform for oral drug delivery. *Journal of Controlled Release,* 81**,** 291-306.

ANDEL, F., LAGARIAS, J. C. & MATHIES, R. A. 1996. Resonance Raman analysis of chromophore structure in the lumi-R photoproduct of phytochrome. *Biochemistry,* 35**,** 15997-16008.

ASHKIN, A. 1992. Forces of a single-beam gradient laser trap on a dielectric sphere in the ray optics regime. *Biophysical Journal,* 61**,** 569.

AU, A. K., HUYNH, W., HOROWITZ, L. F. & FOLCH, A.-Printed 3D Microfluidics. *Angewandte Chemie International Edition*. 2016.

BALTA, D. K., ARSU, N., YAGCI, Y., JOCKUSCH, S. & TURRO, N. J. 2007. Thioxanthone-anthracene: a new photoinitiator for free radical polymerization in the presence of oxygen. *Macromolecules,* 40**,** 4138-4141.

BARRETT, C. B. & GRIZZLE, R. 1999. A holistic approach to sustainability based on pluralism stewardship. *Environmental Ethics,* 21**,** 23-42.

BROUHARD, G. J., SCHEK, H. T. & HUNT, A. J. 2003. Advanced optical tweezers for the study of cellular and molecular biomechanics. *IEEE transactions on biomedical engineering,* 50**,** 121-125.

CHAILLET, N. & RÉGNIER, S. 2013. *Microrobotics for micromanipulation*, John Wiley & Sons.

CHEN, L.-Q. 2002. Phase-field models for microstructure evolution. *Annual review of materials research,* 32**,** 113-140.

CHICHKOV, B. N., MOMMA, C., NOLTE, S., VON ALVENSLEBEN, F. & TÜNNERMANN, A. 1996. Femtosecond, picosecond and nanosecond laser ablation of solids. *Applied Physics A,* 63**,** 109-115.

CHU, S. 1998. Nobel Lecture: The manipulation of neutral particles. *Reviews of Modern Physics,* 70**,** 685.

CICERO, R. L., CHIDSEY, C. E., LOPINSKI, G. P., WAYNER, D. D. & WOLKOW, R. A. 2002. Olefin additions on H-Si (111): Evidence for a surface chain reaction initiated at isolated dangling bonds. *Langmuir,* 18**,** 305-307.

COHEN-TANNOUDJI, C. & GUÉRY-ODELIN, D. 2011. Advances in atomic physics. *World Scientific, Singapore,* 32**,** 36.

CORBIN, E. 2014. *Detection of mass, growth rate, and stiffness of single breast cancer cells using micromechanical sensors.* University of Illinois at Urbana-Champaign.

COSTA, K. D. 2004. Single-cell elastography: probing for disease with the atomic force microscope. *Disease markers,* 19**,** 139-154.

CUMPSTON, B. H., ANANTHAVEL, S. P., BARLOW, S., DYER, D. L., EHRLICH, J. E., ERSKINE, L. L., HEIKAL, A. A., KUEBLER, S. M., LEE, I.-Y. S. & MCCORD-MAUGHON, D. 1999. Two-photon polymerization initiators for three-dimensional optical data storage and microfabrication. *Nature,* 398**,** 51-54.

DE SILVESTRI, S., MAGNI, V., SVELTO, O. & VALENTINI, G. 1990. Lasers with super-Gaussian mirrors. *IEEE Journal of Quantum Electronics,* 26**,** 1500-1509.

DECKER, C., VIET, T. N. T., DECKER, D. & WEBER-KOEHL, E. 2001. UV-radiation curing of acrylate/epoxide systems. *Polymer,* 42**,** 5531-5541.

DEIGLMAYR, J., GROCHOLA, A., REPP, M., MÖRTLBAUER, K., GLÜCK, C., LANGE, J., DULIEU, O., WESTER, R. & WEIDEMÜLLER, M. 2008. Formation of ultracold polar molecules in the rovibrational ground state. *Physical review letters,* 101**,** 133004.

DENIZ, A. A., MUKHOPADHYAY, S. & LEMKE, E. A. 2008. Single-molecule biophysics: at the interface of biology, physics and chemistry. *Journal of the Royal Society Interface,* 5**,** 15-45.

DHOLAKIA, K., REECE, P. & GU, M. 2008. Optical micromanipulation. *Chemical Society Reviews,* 37**,** 42-55.

DISCHER, D. E., BOAL, D. H. & BOEY, S. K. 1998. Simulations of the erythrocyte cytoskeleton at large deformation. II. Micropipette aspiration. *Biophysical Journal,* 75**,** 1584-1597.

EBEWELE, R. O. 2000. *Polymer science and technology*, CRC press.

EGGERS, M. & EHRLICH, D. 1994. A review of microfabricated devices for gene-based diagnostics. *Hematologic pathology,* 9**,** 1-15.

EL-ALI, J., SORGER, P. K. & JENSEN, K. F. 2006. Cells on chips. *Nature,* 442**,** 403-411.

FEYNMAN, R. 2007. Protein Nanomechanics-asStudied by AFM Single-Molecule Force Spectroscopy. *Advanced Techniques in Biophysics,* 10**,** 163.

GOLDSTEIN, J., NEWBURY, D. E., ECHLIN, P., JOY, D. C., ROMIG JR, A. D., LYMAN, C. E., FIORI, C. & LIFSHIN, E. 2012. *Scanning electron microscopy and X-ray microanalysis: a text for biologists, materials scientists, and geologists*, Springer Science & Business Media.

GOMI, H. & KAWATO, M. 1997. Human arm stiffness and equilibrium-point trajectory during multi-joint movement. *Biological cybernetics,* 76**,** 163-171.

GRAESSLEY, W. W. 1982. Entangled linear, branched and network polymer systems—molecular theories. *Synthesis and Degradation Rheology and Extrusion.* Springer.

GRIER, D. G. 2003. A revolution in optical manipulation. *Nature,* 424**,** 810-816.

GUCK, J., ANANTHAKRISHNAN, R., MAHMOOD, H., MOON, T. J., CUNNINGHAM, C. C. & KÄS, J. 2001. The optical stretcher: a novel laser tool to micromanipulate cells. *Biophysical Journal,* 81**,** 767-784.

HENNESSY, J. L. & PATTERSON, D. A. 2011. *Computer architecture: a quantitative approach*, Elsevier.

IKADA, Y. & TSUJI, H. 2000. Biodegradable polyesters for medical and ecological applications. *Macromolecular rapid communications,* 21**,** 117-132.

INOUE, K. & OHTAKA, K. 2013. *Photonic crystals: physics, fabrication and applications*, Springer.

ISOJIMA, T., SUH, S. K., VANDER SANDE, J. B. & HATTON, T. A. 2009. Controlled assembly of nanoparticle structures: spherical and toroidal superlattices and nanoparticle-coated polymeric beads. *Langmuir,* 25**,** 8292-8298.

ITO, K., TANAKA, K., TANAKA, H., IMAI, G., KAWAGUCHI, S. & ITSUNO, S. 1991. Poly (ethylene oxide) macromonomers. 7. Micellar polymerization in water. *Macromolecules,* 24**,** 2348-2354.

JAMES, J. 1976. Specimen, Microscope and Observer; Microscopy in Practice. *Light microscopic techniques in biology and medicine.* Springer.

JUODKAZIS, S., MIZEIKIS, V. & MISAWA, H. 2009. Three-dimensional microfabrication of materials by femtosecond lasers for photonics applications. *Journal of applied physics,* 106**,** 051101.

KINO, G. S. & CORLE, T. R. 1996. *Confocal scanning optical microscopy and related imaging systems*, Academic Press.

KUCKLING, D., VO, C. D. & WOHLRAB, S. E. 2002. Preparation of nanogels with temperature-responsive core and pH-responsive arms by photo-cross-linking. *Langmuir,* 18**,** 4263-4269.

LA PORTA, A. & WANG, M. D. 2004. Optical torque wrench: angular trapping, rotation, and torque detection of quartz microparticles. *Physical review letters,* 92**,** 190801.

LAFRATTA, C. N., FOURKAS, J. T., BALDACCHINI, T. & FARRER, R. A. 2007. Multiphoton fabrication. *Angewandte Chemie International Edition,* 46**,** 6238-6258.

LAKOWICZ, J. R. 2013. *Principles of fluorescence spectroscopy*, Springer Science & Business Media.

LEE, K. S., YANG, D. Y., PARK, S. H. & KIM, R. H. 2006. Recent developments in the use of two-photon polymerization in precise 2D and 3D microfabrications. *Polymers for advanced technologies,* 17**,** 72-82.

LÜ, C. & YANG, B. 2009. High refractive index organic–inorganic nanocomposites: design, synthesis and application. *Journal of Materials Chemistry,* 19**,** 2884-2901.

MA, H., DAVIS, R. H. & BOWMAN, C. N. 2000. A novel sequential photoinduced living graft polymerization. *Macromolecules,* 33**,** 331-335.

MADOU, M. J. 2002. *Fundamentals of microfabrication: the science of miniaturization*, CRC press.

MALAGNINO, N., PESCE, G., SASSO, A. & ARIMONDO, E. 2002. Measurements of trapping efficiency and stiffness in optical tweezers. *Optics communications,* 214**,** 15-24.

MARUO, S. & FOURKAS, J. T. 2008. Recent progress in multiphoton microfabrication. *Laser & Photonics Reviews,* 2**,** 100-111.

MOFFITT, J. R., CHEMLA, Y. R., SMITH, S. B. & BUSTAMANTE, C. 2008. Recent advances in optical tweezers. *Biochemistry,* 77**,** 205.

NEUMAN, K. C. & BLOCK, S. M. 2004. Optical trapping. *Review of scientific instruments,* 75**,** 2787-2809.

NEUMAN, K. C., LIONNET, T. & ALLEMAND, J.-F. 2007. Single-molecule micromanipulation techniques. *Annu. Rev. Mater. Res.,* 37**,** 33-67.

NOVOTNY, L., BIAN, R. X. & XIE, X. S. 1997. Theory of nanometric optical tweezers. *Physical review letters,* 79**,** 645.

OSTENDORF, A. & CHICHKOV, B. N. 2006. Two-photon polymerization: a new approach to micromachining. *Photonics spectra,* 40**,** 72.

OSTERBROCK, D. E. 1958. A Study of Two Comet Tails. *The Astrophysical Journal,* 128**,** 95.

PERCEC, V. & HOLERCA, M. N. 2000. Detecting the shape change of complex macromolecules during their synthesis with the aid of kinetics. A new lesson from biology. *Biomacromolecules,* 1**,** 6-16.

PLANUS, E., FODIL, R., BALLAND, M. & ISABEY, D. 2002. Assessment of mechanical properties of adherent living cells by bead micromanipulation: comparison of magnetic twisting cytometry vs optical tweezers. *Journal of biomechanical engineering,* 124**,** 408-421.

POPMINTCHEV, T., CHEN, M.-C., POPMINTCHEV, D., ARPIN, P., BROWN, S., ALIŠAUSKAS, S., ANDRIUKAITIS, G., BALČIUNAS, T., MÜCKE, O. D. & PUGZLYS, A. 2012. Bright coherent ultrahigh harmonics in the keV x-ray regime from mid-infrared femtosecond lasers. *science,* 336**,** 1287-1291.

RADENOVIC, A. OPTICAL TRAPPING.

RANDALL, C. L., LEONG, T. G., BASSIK, N. & GRACIAS, D. H. 2007. 3D lithographically fabricated nanoliter containers for drug delivery. *Advanced drug delivery reviews,* 59**,** 1547-1561.

REUSS, R. H., CHALAMALA, B. R., MOUSSESSIAN, A., KANE, M. G., KUMAR, A., ZHANG, D. C., ROGERS, J. A., HATALIS, M., TEMPLE, D. & MODDEL, G. 2005. Macroelectronics: Perspectives on technology and applications. *Proceedings of the IEEE,* 93**,** 1239-1256.

RIEF, M., OESTERHELT, F., HEYMANN, B. & GAUB, H. E. 1997. Single molecule force spectroscopy on polysaccharides by atomic force microscopy. *science,* 275**,** 1295-1297.

RUMI, M. & PERRY, J. W. 2010. Two-photon absorption: an overview of measurements and principles. *Advances in Optics and Photonics,* 2**,** 451-518.

SACCONI, L., ROMANO, G., BALLERINI, R., CAPITANIO, M., DE PAS, M., GIUNTINI, M., DUNLAP, D., FINZI, L. & PAVONE, F. 2001. Three-dimensional magneto-optic trap for micro-object manipulation. *Optics letters,* 26**,** 1359-1361.

SEMONIN, O. E., LUTHER, J. M., CHOI, S., CHEN, H.-Y., GAO, J., NOZIK, A. J. & BEARD, M. C. 2011. Peak external photocurrent quantum efficiency exceeding 100% via MEG in a quantum dot solar cell. *science,* 334**,** 1530-1533.

SERBIN, J., OVSIANIKOV, A. & CHICHKOV, B. 2004. Fabrication of woodpile structures by two-photon polymerization and investigation of their optical properties. *Optics Express,* 12**,** 5221-5228.

SHENOY, A. V. 2013. *Rheology of filled polymer systems*, Springer Science & Business Media.

SOLLADIÉ-CAVALLO, A., LUPATTELLI, P. & BONINI, C. 2005. Regio-and stereoselective ring opening of 2, 3-diaryl oxiranes by LiBr/Amberlyst 15: a new stereocontrolled access to 1, 2-diaryl-2-bromo alcohols. *The Journal of organic chemistry,* 70**,** 1605-1611.

SUCCI, S. 2001. *The lattice Boltzmann equation: for fluid dynamics and beyond*, Oxford university press.

SUN, H.-B. & KAWATA, S. 2004. Two-photon photopolymerization and 3D lithographic microfabrication. *NMR• 3D Analysis• Photopolymerization.* Springer.

SURESH, S., SPATZ, J., MILLS, J., MICOULET, A., DAO, M., LIM, C., BEIL, M. & SEUFFERLEIN, T. 2005. Connections between single-cell biomechanics and human disease states: gastrointestinal cancer and malaria. *Acta biomaterialia,* 1**,** 15-30.

SVOBODA, K. & BLOCK, S. M. 1994. Biological applications of optical forces. *Annual review of biophysics and biomolecular structure,* 23**,** 247-285.

TEH, W., DÜRIG, U., DRECHSLER, U., SMITH, C. & GÜNTHERODT, H.-J. 2005. Effect of low numerical-aperture femtosecond two-photon absorption on (SU-8) resist for ultrahigh-aspect-ratio microstereolithography. *Journal of applied physics,* 97**,** 054907.

UREY, H. 2004. Spot size, depth-of-focus, and diffraction ring intensity formulas for truncated Gaussian beams. *Applied optics,* 43**,** 620-625.

VALE, R. D. & MILLIGAN, R. A. 2000. The way things move: looking under the hood of molecular motor proteins. *science,* 288**,** 88-95.

VALEUR, B. & BERBERAN-SANTOS, M. N. 2012. *Molecular fluorescence: principles and applications*, John Wiley & Sons.

VERMA, M. K., MAJUMDER, A. & GHATAK, A. 2006. Embedded template-assisted fabrication of complex microchannels in PDMS and design of a microfluidic adhesive. *Langmuir,* 22**,** 10291-10295.

WANG, M. D., YIN, H., LANDICK, R., GELLES, J. & BLOCK, S. M. 1997. Stretching DNA with optical tweezers. *Biophysical Journal,* 72**,** 1335.

YI, C., LI, C.-W., JI, S. & YANG, M. 2006. Microfluidics technology for manipulation and analysis of biological cells. *Analytica Chimica Acta,* 560**,** 1-23.

YOUSAFZAI, M. S., COCEANO, G., MARIUTTI, A., NDOYE, F., AMIN, L., NIEMELA, J., BONIN, S., SCOLES, G. & COJOC, D. 2016. Effect of neighboring

cells on cell stiffness measured by optical tweezers indentation. *Journal of biomedical optics,* 21**,** 057004-057004.

APPENDICES

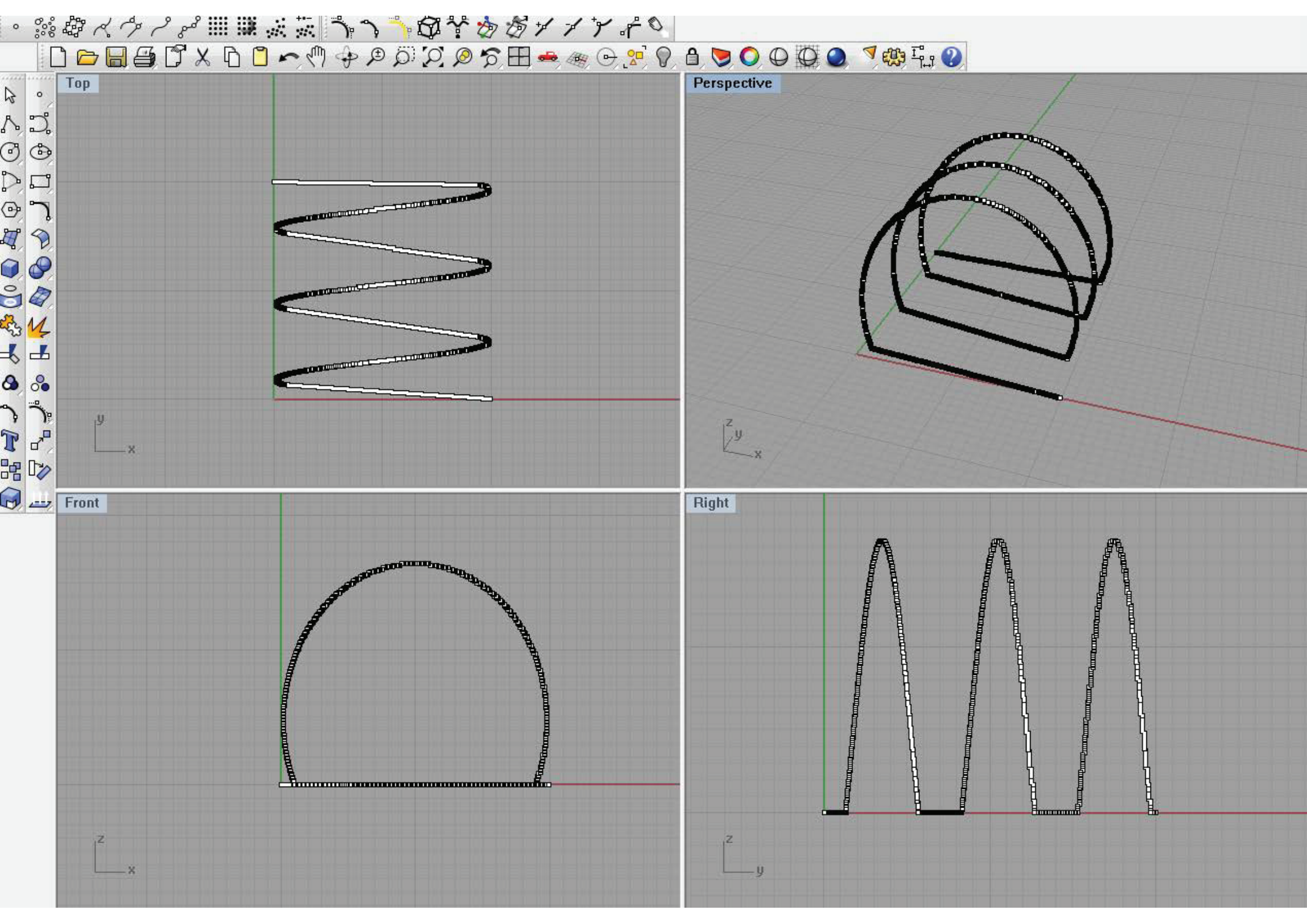
Top
Perspective
Front
Right

May 25, 2016

he videos were recorded for 30 seconds, with 20 fps
he rotation increases with the increasing power.

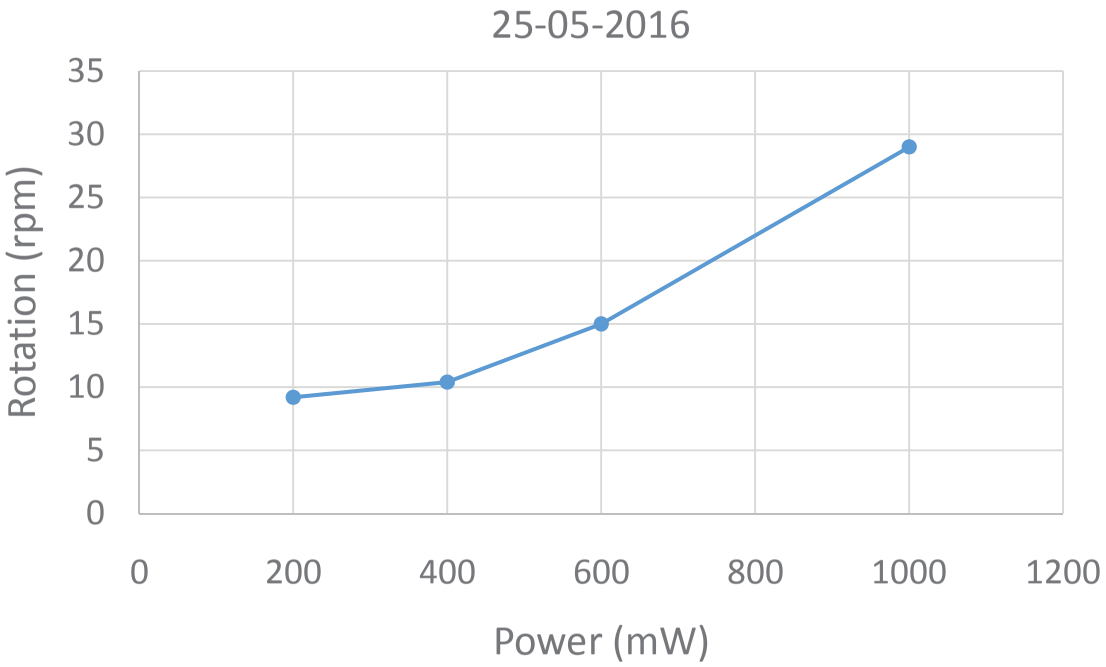

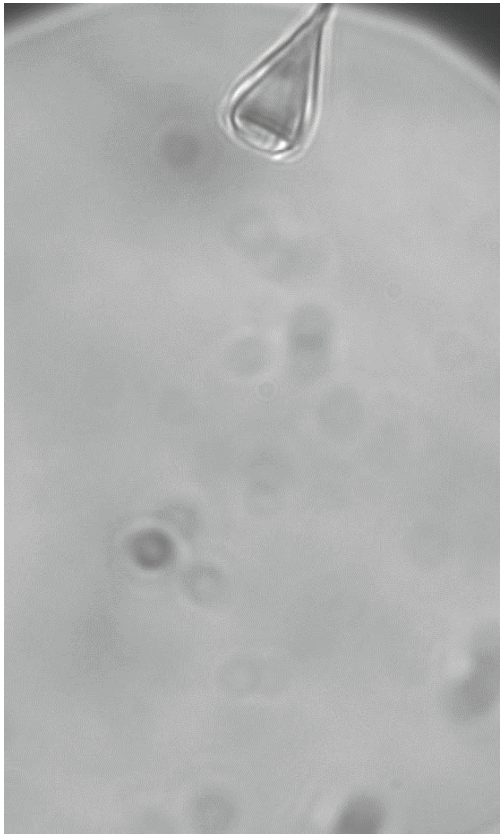

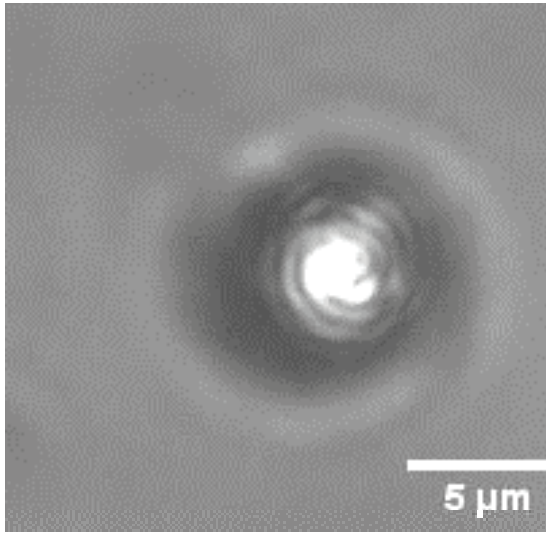

P 400mW

May 31, 2016

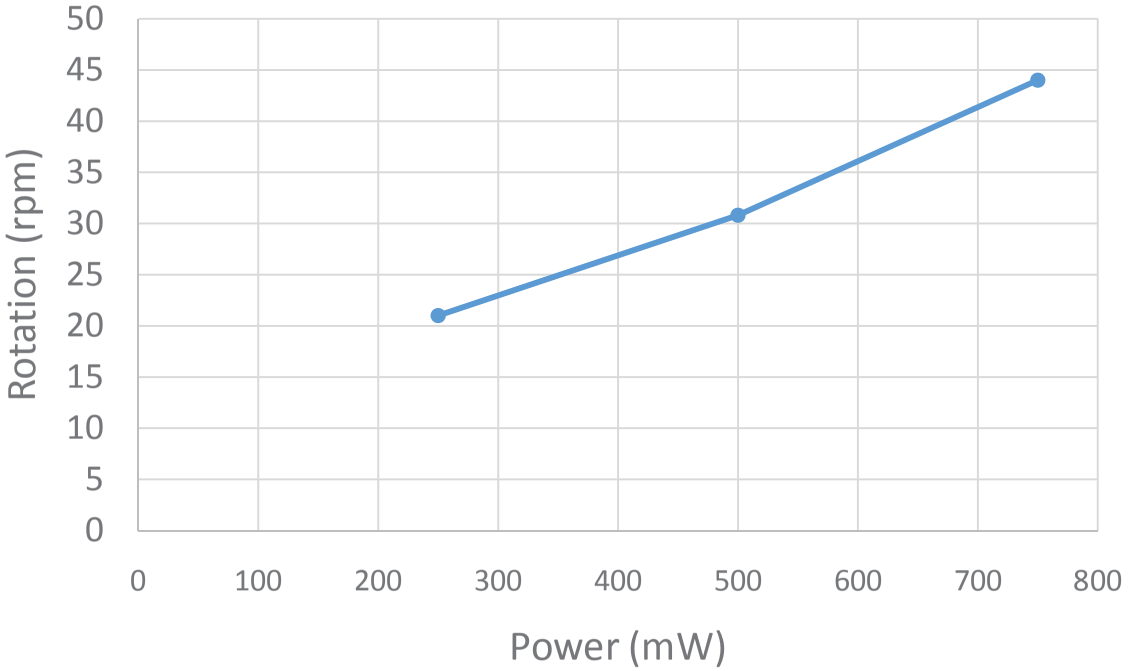

P 500mW

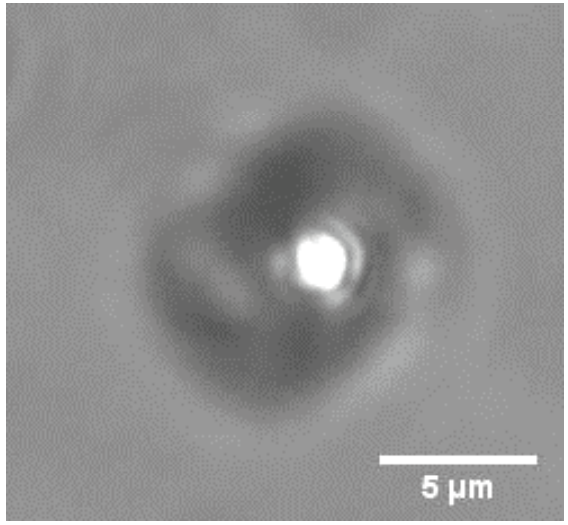

June 09, 2016

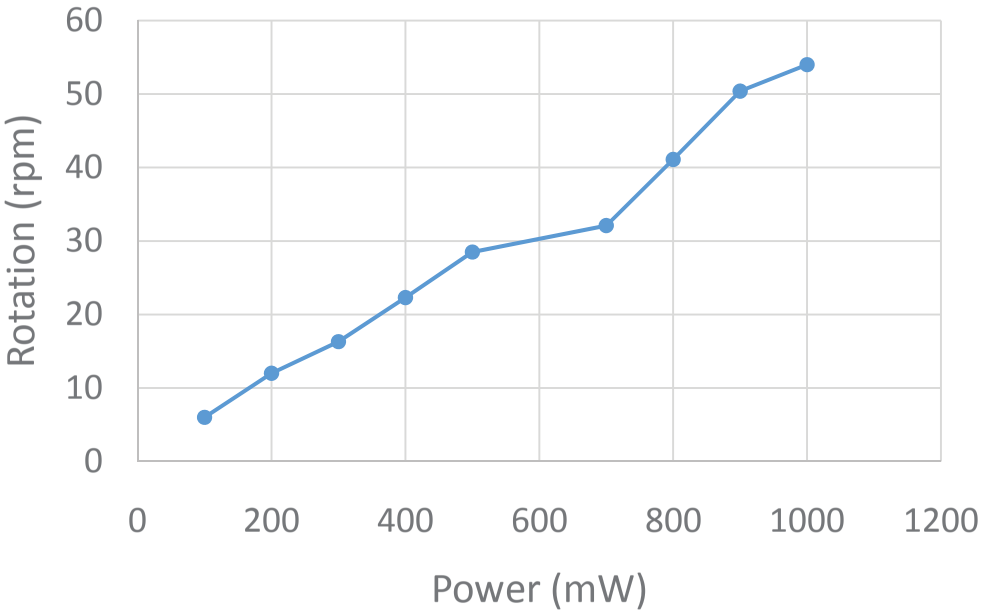

P 500mW

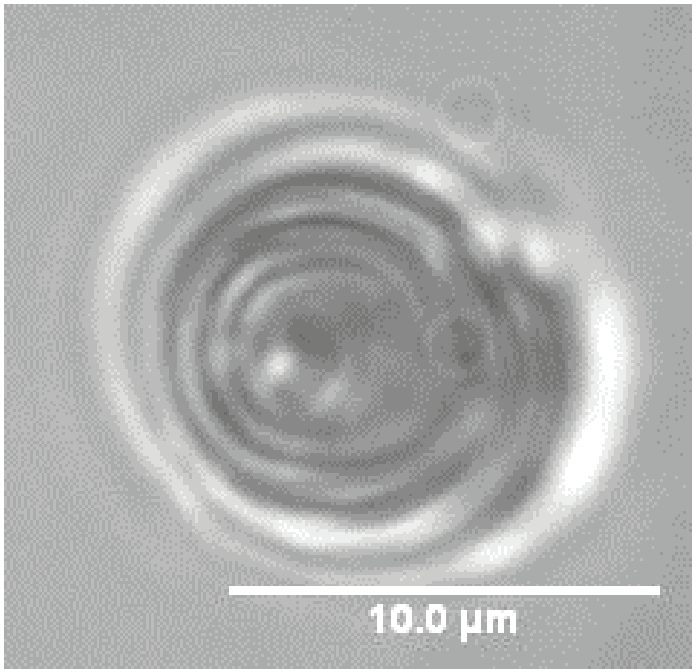

Combined

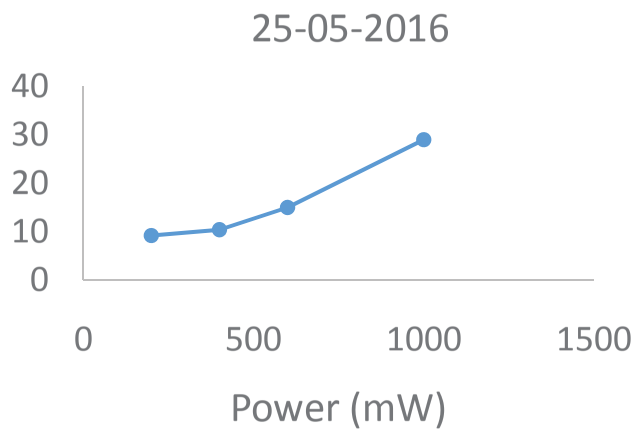

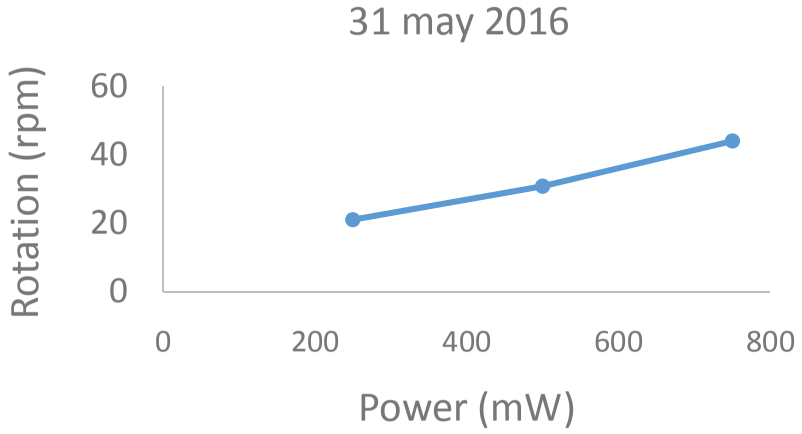

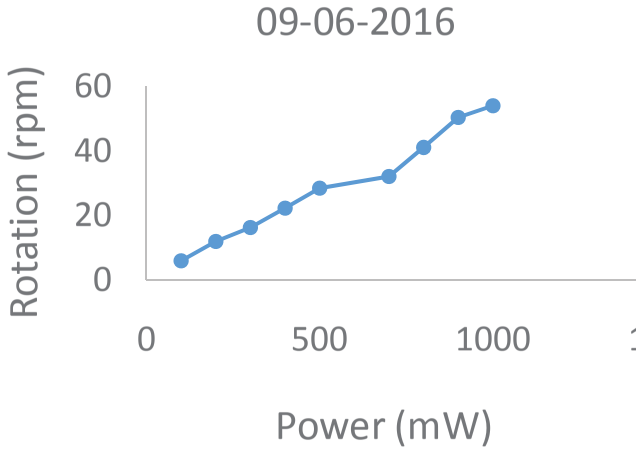

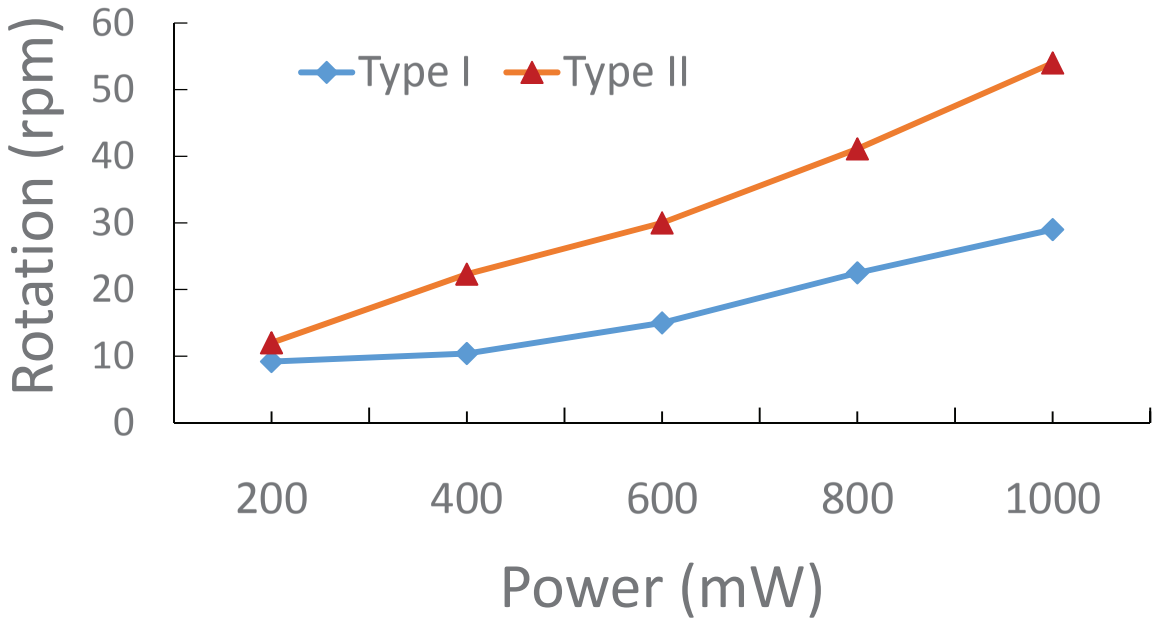

This plot is extracted fro
25-5-2016 and 09-06-20

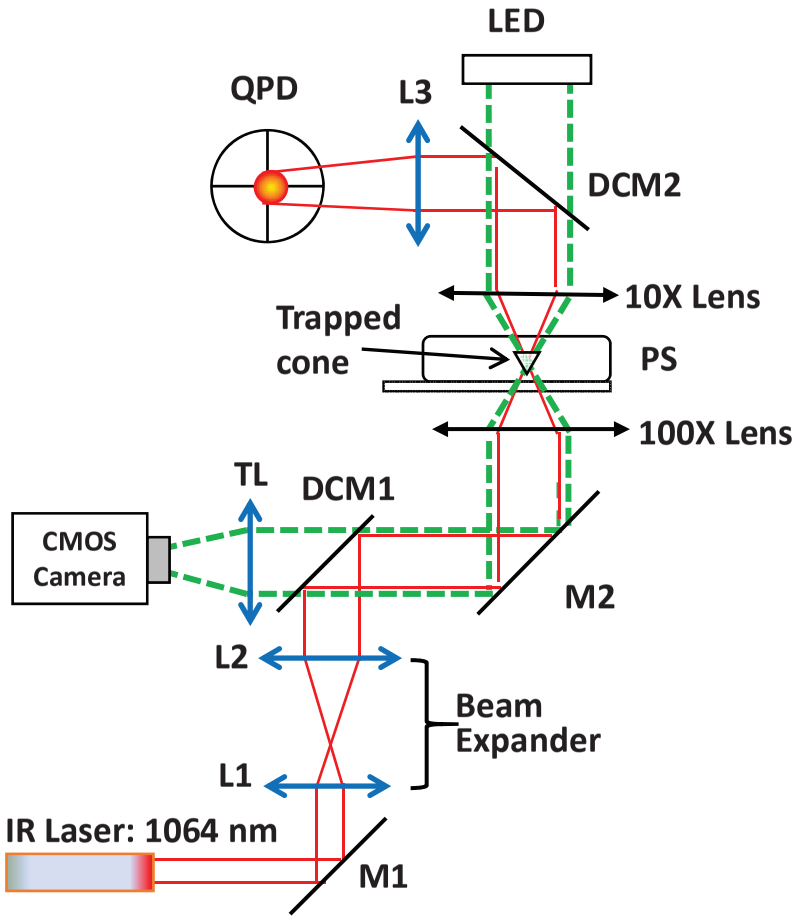
LED
QPD
L3
DCM2
10X Lens
Trapped
cone
PS
100X Lens
TL
DCM1
CMOS
Camera
M2
L2
Beam
Expander
L1
IR Laser: 1064 nm
M1

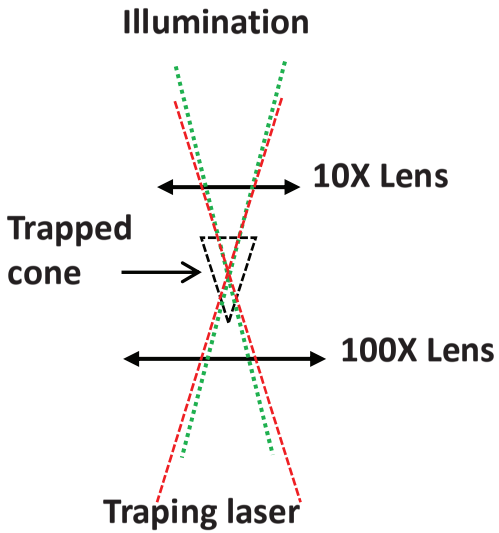
Illumination
10X Lens
Trapped
cone
100X Lens
Traping laser

25-mag-16

Power (mW)	Rotation (rpm)
200	9,2
400	10,4
600	15
1000	29

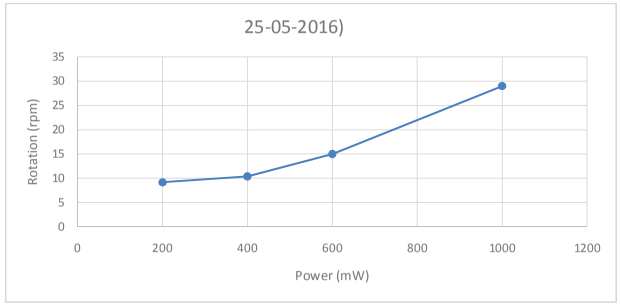

31-mag-16

Power (mW)	Rotation (rpm)
250	21
500	30,8
750	44

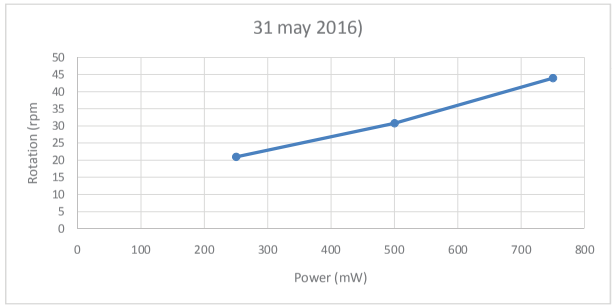

09-06-2016

Power (mW)	Rotation (rpm)
100	6
200	12
300	16,3
400	22,3
500	28,5
700	32,1
800	41,1
900	50,4
1000	54

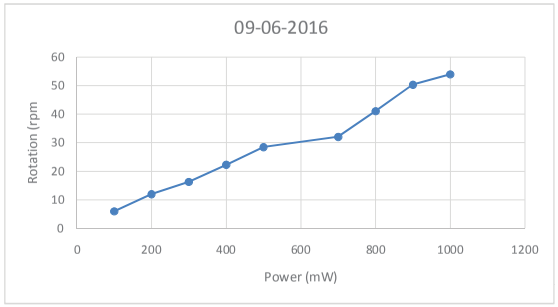

Power (mW)	Type I	Type II
200	9,2	12
400	10,4	22,3
600	15	30
800	22,5	41,1
1000	29	54

middle	25	49,5
intermedia	13	26,6
bottom	7	14,8